Angular values of nonautonomous linear dynamical systems: Part II – Reduction theory and algorithm

Wolf-Jürgen Beyn* Thorsten Hüls*

Abstract. This work focuses on angular values of nonautonomous dynamical systems which have been introduced for general random and (non)autonomous dynamical systems in a previous publication [9]. The angular value of dimension s measures the maximal average rotation which an s-dimensional subspace of the phase space experiences through the dynamics of a discrete-time linear system. Our main results relate the notion of angular value to the well-known dichotomy (or Sacker-Sell) spectrum and its associated spectral bundles. In particular, we prove a reduction theorem which shows that instead of maximizing over all subspaces, it suffices to maximize over so-called trace spaces which have their basis in the spectral fibers. The reduction leads to an algorithm for computing angular values of dimensions one and two. We apply the algorithm to several systems of dimension up to 4 and demonstrate its efficiency to detect the fastest rotating subspace even if it is not dominant under the forward dynamics.

Key words. Nonautonomous dynamical systems, angular value, ergodic average, Sacker-Sell spectrum, numerical approximation.

AMS subject classifications. 37C05, 37E45, 34D09, 65Q10.

1. Introduction.

The concept of angular values was introduced in [9] for (non)autonomous and random linear discrete-time dynamical systems. The purpose of this notion is to measure the average of the largest principle angle between two subspaces at successive times und to maximize this value over all subspaces of a fixed dimension. There is a fundamental difference between such angular values and the well-established theory of Lyapunov exponents which measure the exponential growth or decay of vectors in a dynamical system, see for example [1, Ch.3.2], [8], [29, Suppl.2]. Furthermore, there are important differences to other existing notions which quantify rotations in dynamical systems. Let us mention primarily the rotation number for circle homeomorphisms and for more general maps and flows, see e.g. [2, 13, 29, 30]. While the rotation number measures the oriented angle between vectors and image vectors in two-dimensional subspaces, angular values are based on the principal angles between subspaces which always lie in $[0, \frac{\pi}{2}]$. Even the principal angle between one-dimensional subspaces may differ from the oriented angle between vectors spanning the subspaces. When using principal angles as a measure one loses information about orientation but gains applicability to discrete-time systems in arbitrary dimensions and to subspaces of arbitrary dimension.

While [9] sets out the basic definitions and some general relations between angular values, the construction of an algorithm as well as explicit formulas are restricted to the autonomous and the random case. It is the purpose of this article to provide deeper insight into the general nonautonomous case and to present a robust algorithm.

We consider a nonautonomous linear difference equation of the form

$$u_{n+1} = A_n u_n, \quad A_n \in \mathbb{R}^{d,d}, \quad n \in \mathbb{N}_0 \tag{1.1}$$

and assume throughout this paper that all matrices are invertible and A_n as well as

*Department of Mathematics, Bielefeld University, 33501 Bielefeld, Germany
beyn@math.uni-bielefeld.de, huels@math.uni-bielefeld.de

A_n^{-1} are uniformly bounded. As regards applications, we think of (1.1) to arise from the linearization of a nonlinear (non)autonomous dynamical system along a particular trajectory. In physical terms, we have in mind an object which is carried materially by a time-varying fluid flow and for which data about its position and orientation have been observed at discrete time instances. Then angular values are expected to measure the maximal torsional stress of the object.

The solution operator Φ corresponding to (1.1) is defined by

$$\Phi(n,m) = \begin{cases} A_{n-1} \cdot \ldots \cdot A_m, & \text{for } n > m, \\ I, & \text{for } n = m, \\ A_n^{-1} \cdot \ldots \cdot A_{m-1}^{-1}, & \text{for } n < m. \end{cases}$$

To keep this paper self-contained, some important definitions and estimates of angles from [9] are summarized in Section 2. Our notion of an s-th angular value is based on the averages

$$\frac{1}{n} a_{k+1,k+n}(V), \quad a_{k+1,k+n}(V) = \sum_{j=k+1}^{k+n} \measuredangle(\Phi(j-1,0)V, \Phi(j,0)V), \quad k \geq 0, n \geq 1. \tag{1.2}$$

Here V is an element of the Grassmann manifold $\mathcal{G}(s,d)$ of s-dimensional subspaces of $\mathbb{R}^d$. By $\measuredangle(U,V) \in [0, \frac{\pi}{2}]$ we denote the largest principal angle between two subspaces $U, V \in \mathcal{G}(s,d)$, which can be computed by a singular value decomposition (SVD), see [21, Ch. 6.4.3]. There are several possibilities to pass to a limit in (1.2) and take the supremum over $V \in \mathcal{G}(s,d)$, for example

$$\bar{\theta}_s = \limsup_{n\to\infty} \frac{1}{n} \sup_{V \in \mathcal{G}(s,d)} a_{1,n}(V), \quad \hat{\theta}_s = \sup_{V \in \mathcal{G}(s,d)} \limsup_{n\to\infty} \frac{1}{n} a_{1,n}(V). \tag{1.3}$$

Since the supremum over the Grassmannian occurs either inside or outside the lim sup we call $\bar{\theta}_s$ the sth inner and $\hat{\theta}_s$ the sth outer angular value of the system. Because of the lim sup in (1.3) we give these angular values the additional attribute 'upper', and then define another class of 'lower' angular values where lim inf is used instead. Finally, we consider uniform versions of angular values by first taking the supremum of $a_{k+1,k+n}(V)$ over $k \in \mathbb{N}_0$ and then proceeding as above, see Definition 2.6. This distinguishes between long-time dynamics starting at time zero and longtime dynamics starting at an arbitrary later time. Such a distinction is quite common in the Lyapunov theory when passing from Lyapunov exponents to Bohl exponents or from Lyapunov spectra to dichotomy spectra ([6], [15], [26]). All of the above notions of angular values can be different as examples in [9, Section 3.2] show. At the end of Section 3.2 we will reconsider these examples in view of our reduction theory.

Our numerical methods aim at computing outer angular values for general nonautonomous systems. Recall that the more specific theory and the algorithm from [9, Section 5, 6] are restricted to an autonomous system (1.1), i.e. $A_n = A$ for $n \in \mathbb{N}_0$. In this case all first angular values mentioned above agree and can be computed from orthogonal bases of invariant subspaces which belong to eigenvalues of A of the same modulus. This reduces the numerical effort substantially to a series of Schur decompositions and to one-dimensional optimization.

One major goal of this article is to develop a reduction theorem which generalizes the autonomous results to nonautonomous systems and to subspaces of arbitrary dimension. We tackle this task in Section 3. It turns out that the dichotomy spectrum, also called the Sacker-Sell spectrum [35], and its accompanying spectral bundle take over the role of invariant subspaces from the autonomous case. With every element $V \in \mathcal{G}(s,d)$ we associate a subspace $\mathcal{T}_0(V)$, called the trace space, which has the same dimension as V and which has a basis composed of vectors from the fibers; see (3.16). Our main reduction result Theorem 3.6 then states that the lim sup of $\frac{1}{n}a_{1,n}(V)$ from (1.2) for the given space V agrees with the lim sup of $\frac{1}{n}a_{1,n}(\mathcal{T}_0(V))$ for the trace space. Similar results are derived for the inner angular values ($s = 1$) and for uniform angular values ($s \geq 1$) in Sections 3.3 and 3.4.

The reduction theorem is the basis for the numerical algorithm which we propose in Section 4. Note that angular values are generally not achieved in the most stable or most unstable directions of the trace spaces. Therefore, algorithms, which use forward iteration exclusively, tend to fail since they follow asymptotic dynamics.

Our overall algorithm consists of the following steps:

1. Compute an approximation of the dichotomy spectrum.
2. Compute the corresponding spectral bundles and obtain the trace spaces.
3. Determine the supremum of (1.2) w.r.t. the trace spaces and for large values of n.

The first two tasks are accomplished by using discrete versions of QR-methods from [15] and least squares techniques from [24]. However, by the third step our approach differs substantially from taking QR or SVD decompositions for an overall method, which is common for Lyapunov exponents; see [14],[15]. We apply this algorithm to several models to illustrate various aspects. We begin with a comparison between explicitly known angular values and the output of our algorithm for cases $s = 1, 2$. For the classical Hénon system we illustrate the somewhat slow convergence of the ergodic averages (1.2) as $n \to \infty$ and we discuss their dependence on the initial time k. Further, we give a geometric interpretation of angular values as a measure of the maximal average angle between successive tangent lines to the stable and the unstable fiber bundle within the attractor. In this case the stable fiber rotates faster than the unstable one while the latter is dominant under the forward dynamics. This demonstrates that our reduction procedure is essential in detecting the fastest rotating subspace.

We continue the geometric interpretation of angular values for a 3-dimensional extension of the Hénon system and a 4-dimensional system of coupled oscillators. For the coupled oscillator model we observe that angular values are insensitive to the breakdown of an invariant torus at increasing coupling values. The torus breakdown is known to be related to the ratio of Lyapunov exponents towards vs. inside the torus ([18], [16], [34]). Rather, angular values reflect the rotation of Floquet spaces associated with the periodic orbit approached by the trajectory. This behavior occurs regardless of whether the periodic orbit is imbedded into an invariant torus or not.

2. Basic definitions and properties.

To keep the article self-contained, we summarize in this section some important notions, definitions and results from [9].

2.1. Angles and subspaces.

Let us begin with a useful characterization of the angle between two subspaces V and W of $\mathbb{R}^d$, both having the same dimension s. Principal angles between these subspaces can be computed from the singular values of $V_B^\top W_B$, where

the columns of V_B and $W_B \in \mathbb{R}^{d,s}$ form orthonormal bases of V and W, respectively, see [21, Ch.6.4.3]. The smallest singular value is the cosine of the largest principal angle which we denote by $\measuredangle(V,W)$. We further use the notion

$$\measuredangle(v,w) = \measuredangle(\mathrm{span}(v), \mathrm{span}(w)), \quad v,w \in \mathbb{R}^d, v,w \neq 0$$

in case the subspaces are one-dimensional.

The following characterization of $\measuredangle(V,W)$ turns out to be essential for the analysis of angular values. It provides an alternative to the standard definition in [21, Ch.6.4.3], see [9, Supplementary materials I] for a proof.

Proposition 2.1. *Let $V,W \subseteq \mathbb{R}^d$ be two s-dimensional subspaces. Then the following relation holds*

$$\measuredangle(V,W) = \max_{\substack{v\in V\\ v\neq 0}} \min_{\substack{w\in W\\ w\neq 0}} \measuredangle(v,w) = \arccos\Big(\min_{\substack{v\in V\\ \|v\|=1}} \max_{\substack{w\in W\\ \|w\|=1}} v^\top w\Big).$$

The next proposition summarizes some well-known properties of the Grassmannian

$$\mathcal{G}(s,d) = \{V \subseteq \mathbb{R}^d \text{ is a subspace of dimension } s\},$$

see [21, Ch.6.4.3], [27]. Throughout the paper $\|\cdot\|$ denotes the Euclidean norm of vectors as well as the associated spectral norm of matrices.

Proposition 2.2. *The Grassmannian $\mathcal{G}(s,d)$ is a compact smooth manifold of dimension $s(d-s)$ and a metric space with respect to*

$$d(V,W) = \|P_V - P_W\|,$$

where P_V, P_W are the orthogonal projections onto V and W, respectively. Moreover, the formula

$$d(V,W) = \sin(\measuredangle(V,W)), \quad V,W \in \mathcal{G}(s,d)$$

holds and $\measuredangle(V,W)$ defines an equivalent metric on $\mathcal{G}(s,d)$ satisfying

$$\frac{2}{\pi}\measuredangle(V,W) \leq d(V,W) \leq \measuredangle(V,W).$$

The following lemma from [9, Lemma 2.6] is our main tool to estimate angles of vectors and subspaces in terms of the Euclidean norm.

Lemma 2.3.

i) For any two vectors $v,w \in \mathbb{R}^d$ with $\|v\| < \|w\|$ the following holds

$$\tan^2 \measuredangle(v+w,w) \leq \frac{\|v\|^2}{\|w\|^2 - \|v\|^2}.$$

ii) Let $V \in \mathcal{G}(s,d)$ and $P \in \mathbb{R}^{d,d}$ be such that for some $0 \leq q < 1$

$$\|(I-P)v\| \leq q\|Pv\| \quad \forall v \in V.$$

Then $\dim(V) = \dim(PV)$ and the following estimate holds

$$\measuredangle(V,PV) \leq \frac{q}{(1-q^2)^{1/2}}.$$

Finally, we state a linear algebra result which will provide the basic reduction step in Theorem 3.4. By $\mathcal{R}(P)$ and $\mathcal{N}(P)$ we denote the range and kernel of a matrix P, respectively.

Lemma 2.4. *Let $V \in \mathcal{G}(s,d)$ and let P be a projector in $\mathbb{R}^d$. Furthermore, let Q be any projector defined in $\mathbb{R}^d$ and with range $V \cap \mathcal{R}(P)$. Then the linear map*

$$L = I - P + Q : V \to (I-P)V \oplus (V \cap \mathcal{R}(P)) \tag{2.1}$$

is a bijection and there exists a constant $\rho > 0$ such that

$$\|P(I-Q)v\| \le \rho \|(I-P)(I-Q)v\| \quad \forall v \in V. \tag{2.2}$$

Proof. Note that the sum in (2.1) is direct since $(I-P)V \subseteq \mathcal{N}(P)$. For the same reason, if $Lv = 0$ for some $v \in V$, then $(I-P)v = 0$ and $Qv = 0$ holds. This shows $v \in V \cap \mathcal{R}(P) = \mathcal{R}(Q)$ and $v = Qv = 0$. Thus L is one to one. To show that L is onto, take any $u \in (I-P)V$ and $w \in V \cap \mathcal{R}(P)$. Then we have $u = (I-P)v$ for some $v \in V$, and defining $\tilde{v} = (I-Q)v + w \in V$, we obtain $L\tilde{v} = (I-P)(v+w-Qv) + Qw = (I-P)v + w = u + w$. To show the estimate (2.2) note that $0 = (I-P)(I-Q)v = (I-P)v$ for some $v \in V$ implies $v \in V \cap \mathcal{R}(P) = \mathcal{R}(Q)$ and thus $(I-Q)v = 0 = P(I-Q)v$. Then we obtain (2.2) from the elementary fact that two linear maps $A, B \colon V \to \mathbb{R}^d$ satisfy $\mathcal{N}(B) \subseteq \mathcal{N}(A)$ if and only if there exists a constant $C > 0$ such that $\|Av\| \le C\|Bv\|$ for all $v \in V$. ∎

Remark 2.5. *The last step of the proof is a special case of a result from functional analysis: Let $A, B \colon X \to Y$ be linear bounded operators between Banach spaces X and Y, then A is called relatively bounded by B if there exists a constant $C > 0$ such that $\|Ax\| \le C\|Bx\|$ for all $x \in X$; see [19, Ch.3.7]. The smallest constant of this type is*

$$\rho(A,B) = \inf\{C > 0 : \|Ax\| \le C\|Bx\| \quad \forall x \in X\} = \sup_{Bx \neq 0} \frac{\|Ax\|}{\|Bx\|}. \tag{2.3}$$

If B is Fredholm one can show that A is relatively bounded by B iff $\mathcal{N}(B) \subseteq \mathcal{N}(A)$.

2.2. Definition of angular values. The angular values defined in [9, Section 3.1] always aim at finding the subspace V which maximizes the average angle in (1.2). However, there are several possibilities to let time go to infinity. We will use the attributes 'upper' and 'lower' to distinguish between lim sup and lim inf, and the attributes 'outer' and 'inner' to distinguish between limits taken outside or inside the supremum over the Grassmannian, cf. (1.3). This motivates the first part of the following definition.

Definition 2.6. *Let the nonautonomous system (1.1) be given. For $s \in \{1, \dots, d\}$ define the quantities*

$$a_{m,n}(V) = \sum_{j=m}^{n} \measuredangle(\Phi(j-1,0)V, \Phi(j,0)V) \quad m,n \in \mathbb{N},\ V \in \mathcal{G}(s,d). \tag{2.4}$$

*i) The **upper** resp. **lower** sth **inner angular value** is defined by*

$$\bar{\theta}_s = \limsup_{n\to\infty} \frac{1}{n} \sup_{V \in \mathcal{G}(s,d)} a_{1,n}(V), \quad \underline{\theta}_s = \liminf_{n\to\infty} \frac{1}{n} \sup_{V \in \mathcal{G}(s,d)} a_{1,n}(V). \tag{2.5}$$

ii) The ***upper*** *resp.* ***lower*** *sth* ***outer angular value*** *is defined by*

$$\hat{\theta}_s = \sup_{V\in\mathcal{G}(s,d)} \limsup_{n\to\infty} \frac{1}{n} a_{1,n}(V), \quad \hat{\underline{\theta}}_s = \sup_{V\in\mathcal{G}(s,d)} \liminf_{n\to\infty} \frac{1}{n} a_{1,n}(V).$$

iii) The ***upper*** *resp.* ***lower*** *sth* ***uniform inner angular value*** *is defined by*

$$\begin{aligned} \bar{\theta}_{[s]} &= \lim_{n\to\infty} \frac{1}{n} \sup_{V\in\mathcal{G}(s,d)} \sup_{k\in\mathbb{N}_0} a_{k+1,k+n}(V), \\ \underline{\theta}_{[s]} &= \liminf_{n\to\infty} \frac{1}{n} \sup_{V\in\mathcal{G}(s,d)} \inf_{k\in\mathbb{N}_0} a_{k+1,k+n}(V). \end{aligned} \tag{2.6}$$

iv) The ***upper*** *resp.* ***lower*** *sth* ***uniform outer angular value*** *is defined by*

$$\begin{aligned} \hat{\theta}_{[s]} &= \sup_{V\in\mathcal{G}(s,d)} \lim_{n\to\infty} \frac{1}{n} \sup_{k\in\mathbb{N}_0} a_{k+1,k+n}(V), \\ \hat{\underline{\theta}}_{[s]} &= \sup_{V\in\mathcal{G}(s,d)} \lim_{n\to\infty} \frac{1}{n} \inf_{k\in\mathbb{N}_0} a_{k+1,k+n}(V). \end{aligned}$$

The uniform angular values defined in (iii) and (iv) distinguish between longtime dynamics starting at time zero and longtime dynamics starting at an arbitrary later time. In the stability theory for nonautonomous systems, such a distinction is quite common when passing from Lyapunov exponents to Bohl exponents, see [6], [12, Ch.III.4]. One can show that the limits occurring in Definition 2.6 exist and that the various angular values are related by the diagram below ([9, Lemma 3.3])

$$\begin{array}{ccccccc} \hat{\underline{\theta}}_{[s]} & \leq & \hat{\underline{\theta}}_s & \leq & \hat{\theta}_s & \leq & \hat{\theta}_{[s]} \\ |\wedge & & |\wedge & & |\wedge & & |\wedge \\ \underline{\theta}_{[s]} & \leq & \underline{\theta}_s & \leq & \bar{\theta}_s & \leq & \bar{\theta}_{[s]} \end{array} \tag{2.7}$$

Finally, we note that all inequalities in this diagram can be strict, as suitable examples in [9, Section 3.2] show. However, our numerical computations in Section 4 suggest that such a distinction of angular values is rather exceptional.

3. The dichotomy spectrum and reduction theorems.

We discuss in this section relations between angular values and the dichotomy spectrum. This particularly results in a computational approach for angular values. We start with a brief introduction, cf. [25], of the dichotomy spectrum which is also called the Sacker-Sell spectrum.

3.1. Dichotomy spectrum and trace spaces.

The dichotomy spectrum, see [35] is based on the notion of an exponential dichotomy, cf. [23, 4, 28, 11, 12, 31]. In the following we recall its general definition for a discrete interval $\mathbb{I} \subset \mathbb{Z}$ which is unbounded above, and for a linear system (1.1) which is bounded invertible, i.e. there exists a $C > 0$ such that $\|A_n\|, \|A_n^{-1}\| \leq C$ for all $n \in \mathbb{I}$.

Definition 3.1. *The difference equation* (1.1) *has an* ***exponential dichotomy*** *(**ED** for short) on* $\mathbb{I}$*, if there exist constants* $K > 0, \alpha_s, \alpha_u \in (0,1)$ *and families of projectors* P_n^s*,* $P_n^u := I - P_n^s$*,* $n \in \mathbb{I}$ *such that*

(i) $P_n^{s,u}\Phi(n,m) = \Phi(n,m)P_m^{s,u}$ *for all* $n, m \in \mathbb{I}$.

(ii) For $n, m \in \mathbb{I}$, $n \geq m$ the following estimates hold:

$$\|\Phi(n,m)P_m^s\| \leq K\alpha_s^{n-m}, \quad \|\Phi(m,n)P_n^u\| \leq K\alpha_u^{n-m}.$$

The tuple $(K, \alpha_{s,u}, P_{\mathbb{I}}^{s,u} = (P_n^{s,u})_{n\in\mathbb{I}})$ is called the dichotomy data.

The dichotomy spectrum is constructed, using the scaled equation

$$u_{n+1} = \frac{1}{\gamma}A_n u_n, \quad n \in \mathbb{I}, \tag{3.1}$$

which has the solution operator $\Phi_\gamma(n,m) = \gamma^{m-n}\Phi(n,m)$. Spectrum and resolvent set are defined as follows:

$$\Sigma_{\mathrm{ED}} := \{\gamma > 0 : (3.1) \text{ has no ED on } \mathbb{I}\}, \qquad R_{\mathrm{ED}} := \mathbb{R}^{>0} \setminus \Sigma_{\mathrm{ED}}.$$

The Spectral Theorem [5, Theorem 3.4] provides the decomposition $\Sigma_{\mathrm{ED}} = \bigcup_{i=1}^{\ell} \mathcal{I}_i$ of the dichotomy spectrum into $\ell \leq d$ intervals

$$\mathcal{I}_i = [\sigma_i^-, \sigma_i^+],\ i = 1, \ldots, \ell, \quad \text{where} \quad 0 < \sigma_\ell^- \leq \sigma_\ell^+ < \cdots < \sigma_1^- \leq \sigma_1^+.$$

The intervals $\mathcal{I}_i$, $i = 1, \ldots, \ell$ are called spectral intervals. Correspondingly, the resolvent set is $R_{\mathrm{ED}} = \bigcup_{i=1}^{\ell+1} R_i$ with resolvent intervals

$$R_1 = (\sigma_1^+, \infty), \quad R_i = (\sigma_i^+, \sigma_{i-1}^-),\ i = 2, \ldots, \ell+1 \text{ with } \sigma_{\ell+1}^+ = 0,$$

see Figure 3.1. In case $\sigma_i^- = \sigma_i^+$ for an $i \in \{1, \ldots, \ell\}$ the spectral interval $\mathcal{I}_i$ is an isolated point. For $\gamma \in R_i = (\sigma_i^+, \sigma_{i-1}^-)$ with $i \in \{1, \ldots, \ell+1\}$ the system (3.1) has an ED with

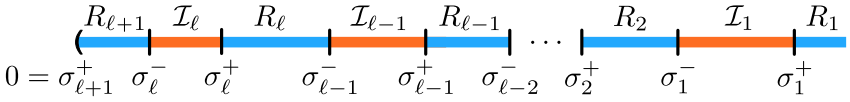

Figure 3.1: Illustration of spectral intervals (orange) and of resolvent intervals (blue).

dichotomy data

$$\left(K\,, \alpha_s(\gamma) = \frac{\sigma_i^+}{\gamma}\,, \alpha_u(\gamma) = \frac{\gamma}{\sigma_{i-1}^-}\,, (P_{n,i}^s, P_{n,i}^u = I - P_{n,i}^s)_{n\in\mathbb{I}}\right). \tag{3.2}$$

The projectors $P_{n,i}^{s,u}$ commute with $\Phi_\gamma(n,m) = \gamma^{m-n}\Phi(n,m)$ as in Definition 3.1 (i) and satisfy for $n \geq m$ the ED-estimates

$$\|\Phi(n,m)P_{m,i}^s\| = \gamma^{n-m}\|\Phi_\gamma(n,m)P_{m,i}^s\| \leq K\gamma^{n-m}\left(\frac{\sigma_i^+}{\gamma}\right)^{n-m} = K(\sigma_i^+)^{n-m},$$

$$\|\Phi(m,n)P_{n,i}^u\| = \gamma^{m-n}\|\Phi_\gamma(m,n)P_{n,i}^u\| \leq K\gamma^{m-n}\left(\frac{\gamma}{\sigma_{i-1}^-}\right)^{n-m} = K\left(\sigma_{i-1}^-\right)^{m-n}.$$

Note that these estimates do not depend on the particular choice of $\gamma \in R_i$. Further, the projectors are uniquely determined and their ranges form a flag of subspaces for $n \in \mathbb{I}$, i.e.

$$\begin{aligned} \{0\} = \mathcal{R}(P^s_{n,\ell+1}) \subseteq \mathcal{R}(P^s_{n,\ell}) \subseteq \quad \cdots \subseteq \mathcal{R}(P^s_{n,1}) = \mathbb{R}^d, \\ \mathbb{R}^d = \mathcal{R}(P^u_{n,\ell+1}) \supseteq \mathcal{R}(P^u_{n,\ell}) \supseteq \quad \cdots \supseteq \mathcal{R}(P^u_{n,1}) = \{0\}. \end{aligned} \tag{3.3}$$

Spectral bundles that correspond to eigenspaces in autonomous systems are defined as follows (see Figure 3.2):

$$\mathcal{W}^i_n := \mathcal{R}(P^s_{n,i}) \cap \mathcal{R}(P^u_{n,i+1}), \quad i = 1, \dots, \ell. \tag{3.4}$$

Note that the dimensions of these spectral bundles $d_i := \dim(\mathcal{W}^i_n)$ for $i = 1, \dots, \ell$ do not depend on $n \in \mathbb{I}$. Alternatively, we may write the ranges of dichotomy projectors in terms of spectral bundles:

$$\mathcal{R}(P^u_{n,i}) = \bigoplus_{j=1}^{i-1} \mathcal{W}^j_n, \quad \mathcal{R}(P^s_{n,i}) = \bigoplus_{j=i}^{\ell} \mathcal{W}^j_n, \quad i = 1, \dots, \ell+1. \tag{3.5}$$

The fiber projector $\mathcal{P}_{n,i}, i = 1, \dots, \ell$ onto $\mathcal{W}^i_n$ along $\bigoplus_{\nu=1,\nu\neq i}^{\ell} \mathcal{W}^\nu_n$ is given by

$$\mathcal{P}_{n,i} = P^s_{n,i}P^u_{n,i+1} = P^u_{n,i+1}P^s_{n,i} = P^s_{n,i} - P^s_{n,i+1} = P^u_{n,i+1} - P^u_{n,i}. \tag{3.6}$$

Spectral bundles satisfy for $i = 1, \dots, \ell$ and $n, m \in \mathbb{I}$ the invariance condition

$$\Phi(n, m)\mathcal{W}^i_m = \mathcal{W}^i_n. \tag{3.7}$$

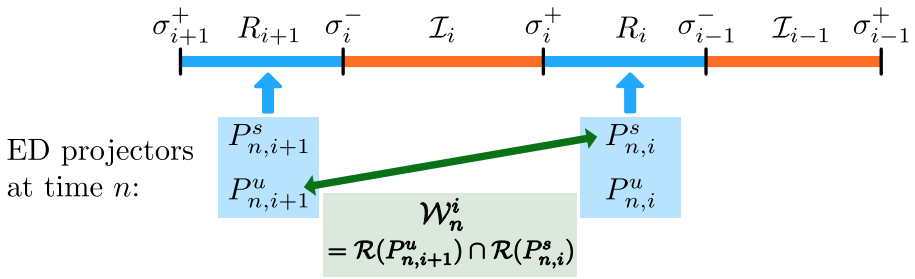

Figure 3.2: Construction of spectral bundles.

For later purposes, we define the following subset of the Grassmannian $\mathcal{G}(s, d)$.

Definition 3.2. *Every element $V \in \mathcal{G}(s, d)$ of the form*

$$V = \bigoplus_{i=1}^{\ell} W_i : W_i \subseteq \mathcal{W}^i_k \text{ (subspace) } i = 1, \dots, \ell, \ \sum_{i=1}^{\ell} \dim W_i = s$$

is called a ***trace space*** *at time k. The set of all trace spaces is denoted by $\mathcal{D}_k(s, d)$.*

Trace spaces depend on the spectral bundle in (3.4) and determine all angular values. Therefore, they form an essential part of the Grassmannian and we will study them in the following subsections.

3.2. Outer angular values and spectral bundles. In the remaining part of this section, we work in the setup $\mathbb{I} = \mathbb{N}_0$. As a first step, we consider a system with an ED and study the forward dynamics $\Phi(j,k)$ of a subspace $V \in \mathcal{G}(s,d)$ starting at an arbitrary time $k \in \mathbb{N}$. Decomposing $V = (\mathcal{R}(P_k^s) \cap V) \oplus \tilde{V}$ where $P_k^u \tilde{V} = P_k^u V$, we see that the stable part $\mathcal{R}(P_k^s) \cap V$ moves to $\Phi(j,k)(\mathcal{R}(P_k^s) \cap V) = \mathcal{R}(P_j^s) \cap \Phi(j,k)V$ because of invariance, while the remaining part $\tilde{V}$ is driven towards the image $\Phi(j,k)P_k^u V = P_j^u \Phi(j,k)V$. Therefore, we expect the image of V to approach $(\mathcal{R}(P_j^s) \cap \Phi(j,k)V) \oplus \Phi(j,k)P_k^u V$ as illustrated in Figure 3.3. This is made precise in the following theorem.

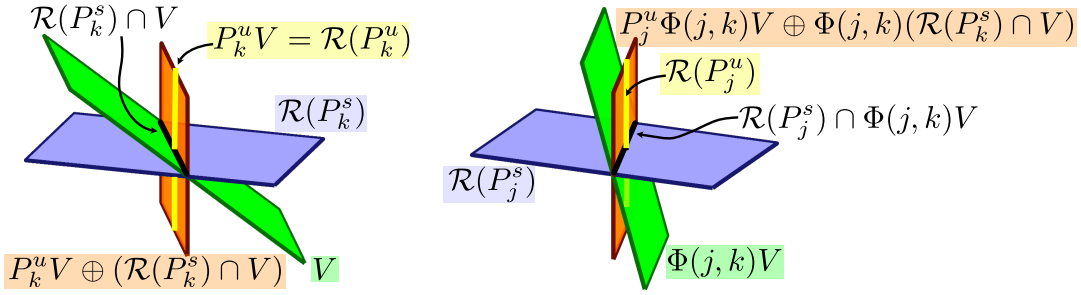

Figure 3.3: A subspace V (green) at time k (left) is driven by the dynamics at time $j > k$ (right) towards the direct sum (orange plane) of its unstable projection (yellow) and the intersection with the stable subspace (black).

Theorem 3.3. *Let the system (1.1) have an exponential dichotomy on $\mathbb{N}_0$ with data $(K, \alpha_{s,u}, P_{\mathbb{N}_0}^{s,u})$. For $k \in \mathbb{N}_0$ and $V \in \mathcal{G}(s,d)$ let*

$$Q_k^s : \mathbb{R}^d \to \mathcal{R}(P_k^s) \cap V \tag{3.8}$$

denote the orthogonal projector onto $\mathcal{R}(P_k^s) \cap V$. Then the quantity (recall (2.3))

$$\rho_k^s(V) = \inf\{C > 0 : \|P_k^s(I - Q_k^s)v\| \le C\|P_k^u(I - Q_k^s)v\| \ \forall v \in V\} < \infty$$

is finite and there exists an index $j_k^s = j_k^s(V)$ such that

$$K^2(\alpha_s\alpha_u)^{j_k^s}\rho_k^s(V) \le \frac{1}{2}. \tag{3.9}$$

For all $j \ge k + j_k^s$ the following estimate holds

$$\measuredangle(\Phi(j,k)V, \Phi(j,k)(P_k^u V \oplus Q_k^s V)) \le \frac{2}{\sqrt{3}} K^2(\alpha_s\alpha_u)^{j-k}\rho_k^s(V). \tag{3.10}$$

Proof. Applying Lemma 2.4 to $P = P_k^s$ and $Q = Q_k^s$ shows that the quantity $\rho_k^s(V)$ is finite. Since $\alpha_s\alpha_u < 1$ there exists an index j_k^s satisfying (3.9). Our goal is to apply Lemma 2.3 (ii) for $j \ge k$ to the s-dimensional subspace $\tilde{V} = \Phi(j,k)V$ and the matrix $\tilde{P} = P_j^u + P_j^s\Phi(j,k)Q_k^s\Phi(k,j)$. First note that Lemma 2.4 and the properties of the solution operator imply

$$\begin{aligned}\Phi(j,k)(P_k^u V \oplus Q_k^s V) &= \Phi(j,k)(P_k^u + Q_k^s)\Phi(k,j)\Phi(j,k)V \\ &= (P_j^u + \Phi(j,k)Q_k^s\Phi(k,j))\Phi(j,k)V = \tilde{P}\tilde{V}.\end{aligned}$$

The exponential dichotomy yields for all $v \in V$ and $j \geq k$

$$\begin{aligned}\|P_k^u v\| &= \|\Phi(k,j)P_j^u\Phi(j,k)(P_k^u v + Q_k^s v)\| \\ &\leq K\alpha_u^{j-k}\|\Phi(j,k)(P_k^u v + Q_k^s v)\| = K\alpha_u^{j-k}\|\tilde{P}\Phi(j,k)v\|, \\ \|(I-\tilde{P})\Phi(j,k)v\| &= \|\Phi(j,k)v - (\Phi(j,k)P_k^u v + \Phi(j,k)P_k^s Q_k^s v)\| \\ &= \|\Phi(j,k)P_k^s(I-Q_k^s)v\| \leq K\alpha_s^{j-k}\|P_k^s(I-Q_k^s)v\|.\end{aligned}$$

Combining these estimates we obtain

$$\begin{aligned}\|(I-\tilde{P})\Phi(j,k)v\| &\leq K\alpha_s^{j-k}\rho_k^s(V)\|P_k^u(I-Q_k^s)v\| = K\alpha_s^{j-k}\rho_k^s(V)\|P_k^u v\| \\ &\leq K^2(\alpha_s\alpha_u)^{j-k}\rho_k^s(V)\|\tilde{P}\Phi(j,k)v\|.\end{aligned} \tag{3.11}$$

By condition (3.9) we can apply Lemma 2.3 (ii) with $q = K^2(\alpha_s\alpha_u)^{j-k}\rho_k^s(V) \leq \frac{1}{2}$ for $j \geq k + j_k^s$ and obtain

$$\measuredangle(\Phi(j,k)V, \Phi(j,k)(P_k^u V \oplus Q_k^s V)) \leq \frac{2K^2}{\sqrt{3}}(\alpha_s\alpha_u)^{j-k}\rho_k^s(V).$$

This proves the estimate (3.10). ∎

In a similar way, we can reverse time and analyze the backwards dynamics of V. For this purpose, let

$$Q_k^u : \mathbb{R}^d \to \mathcal{R}(P_k^u) \cap V \tag{3.12}$$

denote the orthogonal projector onto $\mathcal{R}(P_k^u) \cap V$. Then

$$\rho_k^u(V) = \inf\{C > 0 : \|P_k^u(I-Q_k^u)v\| \leq C\|P_k^s(I-Q_k^u)v\| \ \forall v \in V\} < \infty$$

holds and there exists an index $j_k^u = j_k^u(V)$ such that

$$K^2(\alpha_s\alpha_u)^{j_k^u}\rho_k^u(V) \leq \frac{1}{2}. \tag{3.13}$$

Then we obtain from Lemma 2.3 (ii) the following estimate for all $j \leq k - j_k^u$,

$$\measuredangle(\Phi(j,k)V, \Phi(j,k)(P_k^s V \oplus Q_k^u V)) \leq \frac{2}{\sqrt{3}}K^2(\alpha_s\alpha_u)^{k-j}\rho_k^u(V). \tag{3.14}$$

Theorem 3.3 provides the building block for reducing the analysis of angular values for general subspaces $V \in \mathcal{G}(s,d)$ to specific ones which have a basis consisting of vectors from the spectral bundle (3.4). For a fixed starting time $k \in \mathbb{N}$ and $i = 1, \ldots, \ell$ we recall the projectors $\mathcal{P}_{k,i} = P_{k,i+1}^u P_{k,i}^s : \mathbb{R}^d \to \mathcal{W}_k^i$ from (3.6) and define the orthogonal projectors (cf. (3.3), (3.5), (3.8))

$$Q_{k,i}^s : \mathbb{R}^d \to \mathcal{R}(P_{k,i}^s) \cap V, \quad i = 1, \ldots, \ell. \tag{3.15}$$

With each $V \in \mathcal{G}(s,d)$ we associate a subspace with a fiber basis and defined by

$$\mathcal{T}_k(V) = \bigoplus_{i=1}^{\ell}(\mathcal{P}_{k,i}Q_{k,i}^s V) = \bigoplus_{i=1}^{\ell}(P_{k,i+1}^u(\mathcal{R}(P_{k,i}^s) \cap V)). \tag{3.16}$$

Below we will show $\dim \mathcal{T}_k(V) = s$ and the equality

$$\mathcal{T}_k(V) = \big(\sum_{i=1}^{\ell} \mathcal{P}_{k,i} Q^s_{k,i}\big) V. \tag{3.17}$$

Therefore, $\mathcal{T}_k(V)$ is a trace space at time k in the sense of Definition 3.2. In fact, we have the equality

$$\mathcal{D}_k(s,d) = \{\mathcal{T}_k(V) : V \in \mathcal{G}(s,d)\}, \tag{3.18}$$

since every $V = \bigoplus_{i=1}^{\ell} W_i \in \mathcal{D}_k(s,d)$ with $W_i \subseteq \mathcal{W}^i_k$ satisfies $\mathcal{P}_{k,i} Q^s_{k,i} V = W_i$, $i = 1, \dots, \ell$. Hence every trace space can be found by subsequent projection as in (3.17).

Our main reduction theorem is the following.

Theorem 3.4. *Assume that the difference equation (1.1) has the dichotomy spectrum $\Sigma_{\mathrm{ED}} = \bigcup_{i=1}^{\ell} [\sigma_i^-, \sigma_i^+]$ with fibers $\mathcal{W}^i_k, i = 1 \dots, \ell$ and projectors $\mathcal{P}_{k,i}, i = 1, \dots, \ell$, $k \in \mathbb{N}_0$. Then for every $k \in \mathbb{N}_0$ and $V \in \mathcal{G}(s,d)$, $s = 1, \dots, d$ there exists an index $\overline{j} = \overline{j}(k,V)$ and a constant $C = C(k,V)$ such that for all $j \geq k + \overline{j}$ the following estimate holds*

$$\measuredangle(\Phi(j,k)V, \Phi(j,k)\mathcal{T}_k(V)) \leq C(k,V) \Big(\max_{i=1,\dots,\ell-1} \frac{\sigma^+_{i+1}}{\sigma^-_i} \Big)^{j-k}. \tag{3.19}$$

Remark 3.5. *Note that several of the spaces $\mathcal{P}_{k,i} Q^s_{k,i} V$ occurring in the decomposition (3.16) may be trivial. The following proof will show that one can then omit the corresponding quotients $\frac{\sigma^+_{i+1}}{\sigma^-_i}$ from the maximum in (3.19). Moreover, the proof will provide values for the index $\overline{j}(k,V)$ and the constant $C(k,V)$ in terms of V and the dichotomy data in the resolvent intervals.*

Proof. The main work is to set up inductive steps which apply Theorem 3.3 to Φ_γ for values of γ in successive resolvent intervals.

Step1: Let us first discuss a recursive construction that leads to the trace space (3.17). With every $V \in \mathcal{G}(s,d)$ we associate subspaces $V_i \in \mathcal{G}(s,d)$ and further projectors $\tilde{Q}_{k,i} (i = 1, \dots, \ell+1)$ defined by $V_1 = V$, $\tilde{Q}_{k,1} = I_d$ and then for $i = 1, \dots, \ell$ as follows

$$\begin{aligned} &\tilde{Q}_{k,i+1} : \mathbb{R}^d \to \mathcal{R}(P^s_{k,i+1}) \cap V_i \quad \text{orthogonal projector,} \\ &V_{i+1} = P^u_{k,i+1} V_i \oplus \tilde{Q}_{k,i+1} V_i. \end{aligned} \tag{3.20}$$

Figure 3.4 illustrates this recursion for two characteristic cases. The initial space $V = V_1$ is successively replaced by spaces $V_2, V_3, \dots, V_{\ell+1} =: \mathcal{T}_k(V)$ of the same dimension by working down the flag of subspaces in (3.3). In each step the intersection $\mathcal{R}(P^s_{k,i+1}) \cap V_i$ with the current stable space is kept while the remaining part is replaced by its current unstable projection $P^u_{k,i+1} V_i$.

Note that Lemma 2.4 implies $V_{i+1} = (P^u_{k,i+1} + \tilde{Q}_{k,i+1}) V_i$ and $\dim V_i = \dim V_{i+1}$. In addition, we claim for $i = 1, \dots, \ell$

$$P^u_{k,i+1} V_i = \big(\sum_{\nu=1}^{i} \mathcal{P}_{k,\nu} Q^s_{k,\nu}\big) V, \quad \tilde{Q}_{k,i+1} V_i = Q^s_{k,i+1} V. \tag{3.21}$$

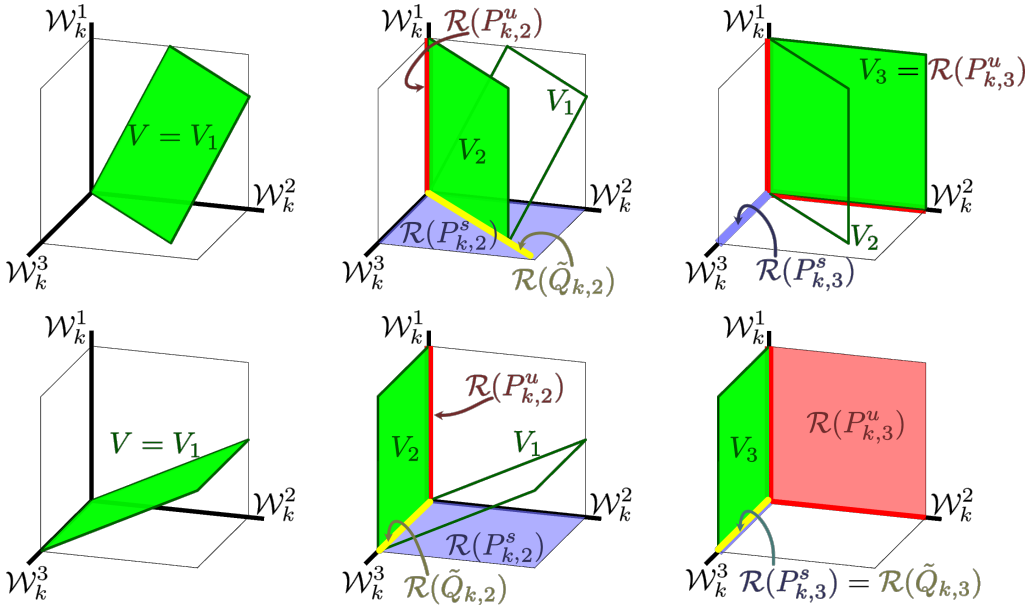

Figure 3.4: Recursive construction of subspaces, cf. (3.20) for two characteristic cases. Upper row: Since V intersects $\mathcal{W}_k^i$ only in $\{0\}$ for any $i \in \{1,2,3\}$, the sequence of subspaces $(V_i)_{i\leq 4}$ is constant for $i \geq 3$, i.e. $V_2 \neq V_3 = V_4$. Lower row: V has a nontrivial intersection with $\mathcal{W}_k^3$ and the sequence of subspaces $(V_i)_{i\leq 4}$ is constant for $i \geq 2$. In both cases, the trace space of V is given as $\mathcal{T}_k(V) = V_3$.

We proceed by induction. First note that (3.3), (3.20) and (3.15) imply $P_{k,1}^s = I_d$, $Q_{k,1}V = \tilde{Q}_{k,1}V_1$. Further, we have by (3.6), (3.20), (3.15)

$$P_{k,2}^u V_1 = \mathcal{P}_{k,1}V, \quad \tilde{Q}_{k,2}V_1 = \mathcal{R}(P_{k,2}^s) \cap V = Q_{k,2}^s V.$$

Assume that (3.21) holds for the index i. Then we obtain from (3.20), (3.5)

$$\begin{aligned}\tilde{Q}_{k,i+2}V_{i+1} &= \mathcal{R}(P_{k,i+2}^s) \cap V_{i+1} = \mathcal{R}(P_{k,i+2}^s) \cap (P_{k,i+1}^u V_i \oplus \tilde{Q}_{k,i+1}V_i) \\ &= \mathcal{R}(P_{k,i+2}^s) \cap \tilde{Q}_{k,i+1}V_i = \mathcal{R}(P_{k,i+2}^s) \cap (\mathcal{R}(P_{k,i+1}^s) \cap V) \\ &= \mathcal{R}(P_{k,i+2}^s) \cap V = Q_{k,i+2}^s V.\end{aligned}$$

Furthermore,

$$\begin{aligned}P_{k,i+2}^u V_{i+1} &= P_{k,i+2}^u (P_{k,i+1}^u V_i \oplus \tilde{Q}_{k,i+1}V_i) \\ &= P_{k,i+2}^u \Big((\sum_{\nu=1}^{i} \mathcal{P}_{k,\nu}Q_{k,\nu}^s)V \oplus Q_{k,i+1}^s V \Big) \\ &= (\sum_{\nu=1}^{i} P_{k,i+2}^u \mathcal{P}_{k,\nu}Q_{k,\nu}^s)V + P_{k,i+2}^u P_{k,i+1}^s Q_{k,i+1}^s V.\end{aligned}$$

From (3.3), (3.5) and (3.6) we have the equalities $P_{k,i+2}^u \mathcal{P}_{k,\nu} = \mathcal{P}_{k,\nu}$ for $\nu \leq i$ and

$P^u_{k,i+2}P^s_{k,i+1} = \mathcal{P}_{k,i+1}$. With $\mathcal{R}(\mathcal{P}_{k,i+1}) \cap \bigoplus_{\nu=1}^{i} \mathcal{W}^\nu_k = \{0\}$ this leads to

$$P^u_{k,i+2}V_{i+1} = \big(\sum_{\nu=1}^{i} \mathcal{P}_{k,\nu}Q^s_{k,\nu}\big)V \oplus \mathcal{P}_{k,i+1}Q^s_{k,i+1}V = \big(\sum_{\nu=1}^{i+1} \mathcal{P}_{k,\nu}Q^s_{k,\nu}\big)V.$$

The last equality needs an argument. The relation "$\supseteq$" is obvious. For the converse we consider $v, w \in V$ and construct $\tilde{v} \in V$ such that

$$\sum_{\nu=1}^{i} \mathcal{P}_{k,\nu}Q^s_{k,\nu}v + \mathcal{P}_{k,i+1}Q^s_{k,i+1}w = \sum_{\nu=1}^{i+1} \mathcal{P}_{k,\nu}Q^s_{k,\nu}\tilde{v}. \tag{3.22}$$

For this purpose set $\tilde{v} = v + Q^s_{k,i+1}(w - v)$ and verify (3.22) by using the equality $\mathcal{P}_{k,\nu}Q^s_{k,\nu}Q^s_{k,i+1}(w-v) = \mathcal{P}_{k,\nu}Q^s_{k,i+1}(w-v) = \mathcal{P}_{k,\nu}P^s_{k,i+1}Q^s_{k,i+1}(w-v) = 0$ for $\nu \le i$. In this way one also obtains the equality of the representations (3.16) and (3.17) via an induction w.r.t. the index i.

Step2: We prove the key estimate (3.19). Let us apply Theorem 3.3 for $i = 1, \dots, \ell$ to the scaled operator Φ_γ with $\gamma \in R_{i+1} = (\sigma^+_{i+1}, \sigma^-_i)$ and $V_i \in \mathcal{G}(s,d)$, $\tilde{Q}_{k,i}$ as defined by (3.20) (recall (3.2) and $\sigma^+_{\ell+1} = 0$). The index $j^s_{k,i}$ is determined by $2K^2\big(\frac{\sigma^+_{i+1}}{\sigma^-_i}\big)^{j^s_{k,i}}\rho^s_{k,i}(V) \le 1$ (cf. (3.9)) where, due to the second equation in (3.21),

$$\rho^s_{k,i}(V) = \inf\{C > 0 : \|P^s_{k,i+1}(I - Q^s_{k,i+1})v\| \le C\|P^u_{k,i+1}(I - Q^s_{k,i+1})v\| \ \forall v \in V\}.$$

Then the estimate (3.10) leads for $j \ge k + j^s_{k,i}$ and $i = 1 \dots, \ell$ to

$$\measuredangle(\Phi_\gamma(j,k)V_i, \Phi_\gamma(j,k)V_{i+1})) \le \frac{2}{\sqrt{3}}K^2\left(\frac{\sigma^+_{i+1}}{\sigma^-_i}\right)^{j-k} \rho^s_{k,i}(V).$$

Since angles do not depend on scalings we can replace Φ_γ by Φ in this estimate. Finally, observe $P^s_{k,\ell+1} = 0$, $Q^s_{k,\ell+1} = 0$ and thus $V_{\ell+1} = P^u_{k,\ell+1}V_\ell = V_\ell = \mathcal{T}_k(V)$ due to (3.21). The triangle inequality then yields for $j - k \ge \bar{j} = \max_{i=1,\dots,\ell} j^s_{k,i}$

$$\begin{aligned}\measuredangle(\Phi(j,k)V, \Phi(j,k)\mathcal{T}_k(V)) &\le \sum_{i=1}^{\ell} \measuredangle(\Phi(j,k)V_i, \Phi(j,k)V_{i+1}) \\ &\le \frac{2K^2}{\sqrt{3}}\left(\max_{i=1,\dots,\ell-1}\frac{\sigma^+_{i+1}}{\sigma^-_i}\right)^{j-k}\sum_{i=1}^{\ell}\rho^s_{k,i}(V). \qquad \blacksquare\end{aligned}$$

Some conclusions of Theorem 3.4 are summarized in Theorem 3.6 below. In particular, we present an important characterization of outer angular values $\hat{\theta}_1$, $\hat{\theta}_1$ if all spectral bundles are one-dimensional.

Theorem 3.6. *Let the assumptions of Theorem 3.4 hold and define the quantities (see (2.4))*

$$a_{1,n}(V) = \sum_{j=1}^{n} \measuredangle(\Phi(j-1,0)V, \Phi(j,0)V) \quad n \in \mathbb{N},\ V \in \mathcal{G}(s,d).$$

Then the following holds for all $V \in \mathcal{G}(s,d)$

$$\limsup_{n\to\infty} \frac{1}{n} a_{1,n}(V) = \limsup_{n\to\infty} \frac{1}{n} a_{1,n}(\mathcal{T}_0(V)), \tag{3.23}$$

and similarly with lim inf *instead of* lim sup. *The outer angular values satisfy*

$$\hat{\theta}_s = \sup_{V\in\mathcal{D}_0(s,d)} \limsup_{n\to\infty} \frac{1}{n} a_{1,n}(V), \quad \hat{\theta}_s = \sup_{V\in\mathcal{D}_0(s,d)} \liminf_{n\to\infty} \frac{1}{n} a_{1,n}(V). \tag{3.24}$$

If $\dim(\mathcal{W}_m^i) = 1$ *for all* $i = 1,\dots,d$ *and* $m \in \mathbb{N}_0$, *then the first lower and upper outer angular values have the form*

$$\begin{aligned} \hat{\theta}_1 &= \max_{i=1,\dots,d} \liminf_{n\to\infty} \frac{1}{n} \sum_{j=1}^{n} \measuredangle(\mathcal{W}_{j-1}^i, \mathcal{W}_j^i), \\ \hat{\theta}_1 &= \max_{i=1,\dots,d} \limsup_{n\to\infty} \frac{1}{n} \sum_{j=1}^{n} \measuredangle(\mathcal{W}_{j-1}^i, \mathcal{W}_j^i). \end{aligned} \tag{3.25}$$

Proof. From the triangle inequality (Proposition 2.2) we obtain

$$\begin{aligned} |a_{1,n}(V) - a_{1,n}(\mathcal{T}_0(V))| &\le \sum_{j=1}^{n} \{\measuredangle(\Phi(j-1,0)V, \Phi(j-1,0)\mathcal{T}_0(V)) \\ &+ \measuredangle(\Phi(j,0)V, \Phi(j,0)\mathcal{T}_0(V))\} \le 2\sum_{j=0}^{n} \measuredangle(\Phi(j,0)V, \Phi(j,0)\mathcal{T}_0(V)). \end{aligned} \tag{3.26}$$

Theorem 3.4 shows that the angles decay geometrically for $j \ge \bar{j}(0,V)$, hence the right-hand side is uniformly bounded by a constant depending on V only. Therefore (3.23) follows, and (3.24) is an immediate consequence by taking the supremum with respect to V.

In the case $s = 1$ and $\dim(\mathcal{W}_m^i) = 1$ for $i = 1,\dots,d$ the set $\mathcal{D}_0(1,d) = \{\mathcal{W}_0^i : i = 1,\dots,d\}$ becomes finite. Moreover, we have $\Phi(j,0)\mathcal{W}_0^i = \mathcal{W}_j^i$ by the invariance condition (3.7). Thus, the formula (3.24) simplifies to (3.25). ∎

In view of Theorem 3.4, we revisit crucial examples from [9, Section 3.2]. The first model is defined for $n \in \mathbb{N}_0$ and $0 \le \varphi_0 < \varphi_1 \le \frac{\pi}{2}$ by

$$A_n = \begin{cases} \begin{pmatrix} \cos(\varphi_0) & -\sin(\varphi_0) \\ \sin(\varphi_0) & \cos(\varphi_0) \end{pmatrix}, & \text{for } n = 0 \vee n \in \bigcup_{\ell=1}^{\infty} [2^{2\ell-1}, 2^{2\ell} - 1] \cap \mathbb{N}, \\ \begin{pmatrix} \cos(\varphi_1) & -\sin(\varphi_1) \\ \sin(\varphi_1) & \cos(\varphi_1) \end{pmatrix}, & \text{otherwise.} \end{cases}$$

For this example, upper and lower angular values do not coincide in general, more precisely, the diagram (2.7) now reads

$$\begin{array}{ccccccc} \underset{\frown}{\theta}_{[1]} & < & \underset{\frown}{\theta}_1 & < & \hat{\theta}_1 & < & \hat{\theta}_{[1]} \\ \| & & \| & & \| & & \| \\ \underline{\theta}_{[1]} & < & \underline{\theta}_1 & < & \bar{\theta}_1 & < & \bar{\theta}_{[1]}. \end{array}$$

For the second example, defined for $n \in \mathbb{N}_0$ by

$$A_n := \begin{cases} \left(\begin{smallmatrix} -1 & 0 \\ 0 & 1 \end{smallmatrix}\right), & \text{for } n \in \bigcup_{\ell=1}^{\infty} [2 \cdot 2^\ell - 4, 3 \cdot 2^\ell - 5], \\ \left(\begin{smallmatrix} 1 & 0 \\ 0 & \frac{1}{2} \end{smallmatrix}\right), & \text{otherwise} \end{cases}$$

inner and outer angular values differ, i.e. the diagram (2.7) turns into

$$\begin{array}{ccccccc} \hat{\underline{\theta}}_{[1]} & = & \hat{\underline{\theta}}_1 & = & \hat{\theta}_1 & = & \hat{\theta}_{[1]} \\ \| & & \wedge & & \wedge & & \wedge \\ \underline{\theta}_{[1]} & < & \underline{\theta}_1 & < & \bar{\theta}_1 & < & \bar{\theta}_{[1]}. \end{array}$$

The dichotomy spectrum of the first example is given by $\Sigma_{\mathrm{ED}} = \{1\}$ and for the second example, we obtain $\Sigma_{\mathrm{ED}} = [\frac{1}{2}, 1]$. In both cases $\mathcal{W}_k^1 = \mathbb{R}^2$ for all $k \in \mathbb{N}$. Thus one-dimensional trace spaces agree with the given space. In particular, the detection of angular values cannot be reduced by Theorem 3.4 and Theorem 3.6 to lower dimensional spaces.

3.3. Inner angular values and spectral bundles. Inner angular values are more difficult to handle, both numerically and theoretically, since the supremum over all subspaces is taken before going to the limit. For general dimensions we do not have a result comparable to Theorem 3.4. However, for one-dimensional subspaces a reduction is possible under a uniformity condition. Recall from (2.4) the notion

$$a_{m,n}(v) = \sum_{j=m}^{n} \measuredangle(\Phi(j-1,0)v, \Phi(j,0)v) \quad m,n \in \mathbb{N},\ v \in \mathbb{R}^d, v \neq 0 \tag{3.27}$$

with $a_{m,n}(v) = 0$ for $m > n$. For a subspace $V \subseteq \mathbb{R}^d$ we introduce the quantity

$$\overline{\theta}_1(V) = \limsup_{n\to\infty} \sup_{v\in V, v\neq 0} \frac{a_{1,n}(v)}{n}.$$

Note that $\overline{\theta}_1(V)$ is the maximum angular value for all one-dimensional subspaces of V. In case $V = \mathbb{R}^d$ this value agree with $\overline{\theta}_1$ as defined in (2.5).

Theorem 3.7. *Let the assumptions of Theorem 3.4 hold. Further assume that the inner and the uniform inner angular values (cf. (2.5), (2.6) and (2.7)) agree within each fiber, i.e. for $i = 1, \dots, \ell$ the following holds*

$$\overline{\theta}_1(\mathcal{W}_0^i) = \lim_{n\to\infty} \frac{1}{n} \sup_{v\in\mathcal{W}_0^i, v\neq 0} \sup_{k\in\mathbb{N}_0} a_{k+1,k+n}(v). \tag{3.28}$$

Then the first inner angular value $\overline{\theta} = \overline{\theta}_1(\mathbb{R}^d)$ satisfies

$$\overline{\theta}_1 = \max_{i=1,\dots,\ell} \overline{\theta}_1(\mathcal{W}_0^i).$$

Proof. The main step is to show for $i = 1, \dots, \ell$

$$\overline{\theta}_1(\mathcal{R}(P_{0,i}^s)) \leq \max\left(\overline{\theta}_1(\mathcal{W}_0^i), \overline{\theta}_1(\mathcal{R}(P_{0,i+1}^s))\right). \tag{3.29}$$

Since $P^s_{0,1} = I_d$, $P^s_{0,\ell+1} = 0$ and $\sup\emptyset = 0$, we obtain by induction

$$\overline{\theta}_1(\mathbb{R}^d) \le \max_{i=1,\dots,\ell} \overline{\theta}_1(\mathcal{W}^i_0).$$

The converse inequality "$\ge$" is obvious, hence our assertion is proved.

In the following we choose $j_\star$ such that (cf. (3.19))

$$2K^2 q^{j_\star} \le 1, \quad \text{where} \quad q := \max_{i=1,\dots,\ell} \frac{\sigma^+_{i+1}}{\sigma^-_i} < 1.$$

For the proof of (3.29) it is enough to consider $v \in \mathcal{R}(P^s_{0,i})$ with $v \notin \mathcal{R}(P^s_{0,i+1})$ and $v \notin \mathcal{W}^i_0$. Figure 3.5 illustrates the idea of the proof. Vectors v close to but not in $\mathcal{R}(P^s_{0,i+1})$ may spend arbitrarily large time near $\mathcal{R}(P^s_{0,i+1})$ until finally converging to $\mathcal{R}(P^u_{0,i+1})$. There is an exponentially growing initial phase switching at some index $k_\star$ to an exponentially decreasing final phase. Though the switching point $k_\star$ depends on v our uniformity assumption will allow estimates independent of v. We choose $\gamma \in R_{i+1}$

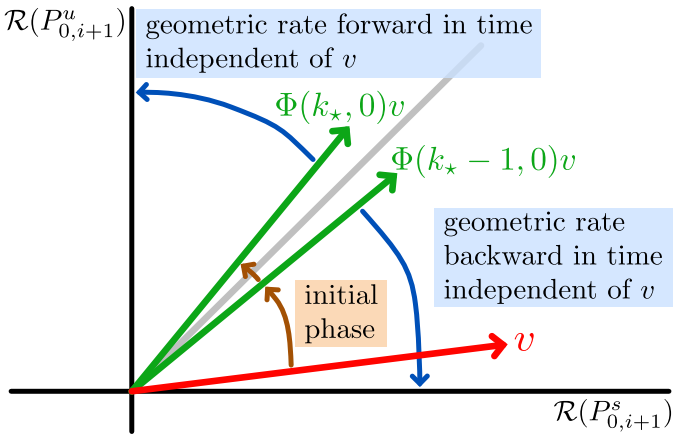

Figure 3.5: Idea of proof for Theorem 3.7. First, we construct a v-dependent index $k_\star$, such that $\Phi(k_\star, 0)v$ is just above the diagonal. Then, we exploit geometric convergence forward resp. backward in time for proving v-independent estimates.

and apply Theorem 3.3 to Φ_γ and $V = \operatorname{span}(v)$ as in Step 2 of the proof of Theorem 3.4. Note that the projector $Q^s_{0,i+1} : \mathbb{R}^d \to \mathcal{R}(P^s_{0,i+1}) \cap V$ from (3.15) is trivial since V is one-dimensional and $v \notin \mathcal{R}(P^s_{0,i+1})$. Moreover, by (3.6) we have $\mathcal{P}_{0,i}v = P^u_{0,i+1}P^s_{0,i}v = P^u_{0,i+1}v \neq 0$. Therefore, we can invoke inequality (3.11) from the proof of Theorem 3.3 with $\tilde{P} = P^u_{k,i+1}$, $\rho^s_k(v) = \frac{\|P^s_{0,i+1}v\|}{\|P^u_{0,i+1}v\|}$, $\alpha_s\alpha_u \le q$. This shows

$$\|P^s_{k,i+1}\Phi_\gamma(k,0)v\| \le K^2 q^k \rho^s_k(v) \|P^u_{k,i+1}\Phi_\gamma(k,0)v\| \quad \forall k \in \mathbb{N}_0.$$

We conclude that the following index, depending on v, exists

$$k_\star = k_\star(v) = \min\{k \in \mathbb{N}_0 : \|P^s_{k,i+1}\Phi_\gamma(k,0)v\| \le \|P^u_{k,i+1}\Phi_\gamma(k,0)v\|\}.$$

Applying Theorem 3.3 once more to Φ_γ and $V = \operatorname{span}(\Phi_\gamma(k_\star, 0)v)$ then shows for $j \geq k_\star + j_\star$

$$\begin{aligned}&\measuredangle(\Phi(j,k_\star)\Phi(k_\star,0)v, \Phi(j,k_\star)P^u_{k_\star,i+1}\Phi(k_\star,0)v)\\ &= \measuredangle(\Phi(j,0)v, \Phi(j,0)P^u_{0,i+1}v) \leq \frac{2K^2}{\sqrt{3}} q^{j-k_\star}.\end{aligned}$$

Next we estimate angles for $j \leq k_\star$ by invoking (3.14) with $k = k_\star - 1$ and $V = \operatorname{span}(\Phi_\gamma(k_\star - 1, 0)v)$. Since $v \notin \mathcal{W}^i_0$ the projector in (3.12) is trivial, and (3.13) holds by the choice of $j_\star$. Hence we obtain for $0 \leq j \leq k_\star - 1 - j_\star$

$$\begin{aligned}&\measuredangle(\Phi(j,k_\star-1)\Phi(k_\star-1,0)v, \Phi(j,k_\star)P^s_{k_\star,i+1}\Phi(k_\star,0)v)\\ &= \measuredangle(\Phi(j,0)v, \Phi(j,0)P^s_{0,i+1}v) \leq \frac{2K^2}{\sqrt{3}} q^{k_\star-1-j}.\end{aligned}$$

Combining these estimates with the triangle inequality we find with suitable constants C independent of n, j, v,

$$\begin{aligned}\frac{a_{1,n}(v)}{n} &= \frac{1}{n}\sum_{j=1}^{n} \measuredangle(\Phi(j-1,0)v, \Phi(j,0)v)\\ &\leq \frac{1}{n}\Big[\Big\{\sum_{j=1}^{k_\star-1-j_\star} + \sum_{j=k_\star+1+j_\star}^{n}\Big\}\measuredangle(\Phi(j-1,0)v, \Phi(j,0)v) + (2j_\star+1)\frac{\pi}{2}\Big]\\ &\leq \frac{1}{n}\Big[\frac{4K^2}{\sqrt{3}}\Big(\sum_{j=0}^{k_\star-1-j_\star} q^{k_\star-1-j} + \sum_{j=k_\star}^{n} q^{j-k_\star}\Big) + C\\ &\quad + \sum_{j=1}^{k_\star} \measuredangle(\Phi(j-1,0)P^s_{0,i+1}v, \Phi(j,0)P^s_{0,i+1}v)\\ &\quad + \sum_{j=k_\star+1}^{n} \measuredangle(\Phi(j-1,0)P^u_{0,i+1}v, \Phi(j,0)P^u_{0,i+1}v)\Big]\\ &\leq \frac{1}{n}\left[C + a_{1,k_\star}(P^s_{0,i+1}v) + a_{k_\star+1,n}(P^u_{0,i+1}v)\right].\end{aligned} \tag{3.30}$$

Given $\varepsilon > 0$, assumption (3.28) yields a number $n_0 = n_0(\varepsilon)$ such that

$$\begin{aligned}&\frac{1}{n}\sup_{k\in\mathbb{N}_0}\sup_{v\in\mathcal{W}^i_0} a_{k+1,k+n}(v) \leq \overline{\theta}_1(\mathcal{W}^i_0) + \varepsilon, \quad \forall n \geq n_0,\\ &\frac{1}{n}\sup_{v\in\mathcal{R}(P^s_{0,i+1})} a_{1,n}(v) \leq \overline{\theta}_1(\mathcal{R}(P^s_{0,i+1})) + \varepsilon, \quad \forall n \geq n_0.\end{aligned} \tag{3.31}$$

Thus we have

$$a_{k_\star+1,n}(P^u_{0,i+1}v) \leq \begin{cases}(n-k_\star)(\overline{\theta}_1(\mathcal{W}^i_0) + \varepsilon), & \text{if } n - k_\star \geq n_0,\\ n_0\frac{\pi}{2}, & \text{if } n - k_\star < n_0,\end{cases}$$

$$a_{1,k_\star}(P^s_{0,i+1}v) \leq \begin{cases}k_\star(\overline{\theta}_1(\mathcal{R}(P^s_{0,i+1})) + \varepsilon), & \text{if } k_\star \geq n_0,\\ n_0\frac{\pi}{2}, & \text{if } k_\star < n_0.\end{cases}$$

Summing up, we obtain for $n \geq n_0(\varepsilon)$,

$$\frac{a_{1,n}(v)}{n} \leq \frac{1}{n}\big[\min(k_\star, n)(\overline{\theta}_1(\mathcal{R}(P^s_{0,i+1})) + \varepsilon) + (n - \min(n, k_\star))(\overline{\theta}_1(\mathcal{W}^i_0) + \varepsilon) \\ + C + n_0\pi\big] \leq \max(\overline{\theta}_1(\mathcal{W}^i_0), \overline{\theta}_1(\mathcal{R}(P^s_{0,i+1}))) + \varepsilon + \frac{1}{n}(C + n_0\pi).$$

Finally, the assertion (3.29) follows by taking the supremum over v and making the last term small for n sufficiently large. ∎

3.4. Uniform angular values and spectral bundles. In this section we extend Theorem 3.6 and Theorem 3.7 to uniform outer and inner angular values. As before, we show that it is enough to compute angular values for subspaces which have their basis in the fibers induced by the dichotomy spectrum. Since we deal with uniform angular values a uniformity condition like (3.28) is no longer needed.

Theorem 3.8. *Let the assumptions of Theorem 3.4 hold. Then the uniform outer angular values $\hat{\theta}_{[s]}, \hat{\underline{\theta}}_{[s]}$, $s = 1, \dots, d$, can be represented with the partial sums (2.4) and the set of trace spaces (3.18) as follows:*

$$\hat{\theta}_{[s]} = \sup_{V \in \mathcal{D}_0(s,d)} \lim_{n\to\infty} \sup_{k \in \mathbb{N}_0} \frac{1}{n} a_{k+1,k+n}(V), \tag{3.32}$$

$$\hat{\underline{\theta}}_{[s]} = \sup_{V \in \mathcal{D}_0(s,d)} \lim_{n\to\infty} \inf_{k \in \mathbb{N}_0} \frac{1}{n} a_{k+1,k+n}(V). \tag{3.33}$$

With the partial sums from (3.27), the first uniform inner angular value satisfies

$$\overline{\theta}_{[1]} = \max_{i=1,\dots,\ell} \overline{\theta}_{[1]}(\mathcal{W}^i_0), \quad \text{where} \quad \overline{\theta}_{[1]}(V) = \lim_{n\to\infty} \sup_{v \in V} \sup_{k \in \mathbb{N}_0} \frac{1}{n} a_{k+1,k+n}(v). \tag{3.34}$$

Proof. Recall $a_{m,n}(V)$ from (2.4) and use (3.26), (3.19) to find that $V \in \mathcal{G}(s,d)$ satisfies with some constant C depending on V but not on k, n,

$$\begin{aligned} |a_{k+1,k+n}(V) - a_{k+1,k+n}(\mathcal{T}_0(V))| &\leq 2\sum_{j=k}^{k+n} \measuredangle(\Phi(j,0)V, \Phi(j,0)(\mathcal{T}_0(V))) \\ &\leq 2C(0,V)\sum_{j=k}^{k+n} q^{j-k} \leq C. \end{aligned} \tag{3.35}$$

Given $\varepsilon > 0$, choose n_0 such that for $n \geq n_0$

$$\Big|\frac{1}{n}\sup_{k\in\mathbb{N}_0} a_{k+1,k+n}(V) - \lim_{m\to\infty}\frac{1}{m}\sup_{k\in\mathbb{N}_0} a_{k+1,k+m}(V)\Big| \leq \varepsilon.$$

Then select $k(n) \in \mathbb{N}_0$ such that $\frac{1}{n}|a_{k(n)+1,k(n)+n}(V) - \sup_{k\in\mathbb{N}_0} a_{k+1,k+n}(V)| \leq \varepsilon$ holds for $n \geq n_0$. This implies

$$\Big|\frac{1}{n}a_{k(n)+1,k(n)+n}(V) - \lim_{m\to\infty}\frac{1}{m}\sup_{k\in\mathbb{N}_0} a_{k+1,k+m}(V)\Big| \leq 2\varepsilon, \quad n \geq n_0.$$

With (3.35) we obtain for $n \geq n_0$

$$\begin{aligned}\lim_{m\to\infty} \frac{1}{m} \sup_{k\in\mathbb{N}_0} a_{k+1,k+m}(V) &\leq \frac{1}{n} a_{k(n)+1,k(n)+n}(V) + 2\varepsilon \\ &\leq \frac{C}{n} + \frac{1}{n} a_{k(n)+1,k(n)+n}(\mathcal{T}_0(V)) + 2\varepsilon \\ &\leq \frac{C}{n} + \frac{1}{n} \sup_{k\in\mathbb{N}_0} a_{k+1,k+n}(\mathcal{T}_0(V)) + 2\varepsilon.\end{aligned}$$

As $n \to \infty$ this shows

$$\lim_{n\to\infty} \frac{1}{n} \sup_{k\in\mathbb{N}_0} a_{k+1,k+n}(V) \leq 2\varepsilon + \lim_{n\to\infty} \frac{1}{n} \sup_{k\in\mathbb{N}_0} a_{k+1,k+n}(\mathcal{T}_0(V)).$$

A corresponding inequality with V and $\mathcal{T}_0(V)$ exchanged, is proved in the same manner, and (3.32) follows by taking the supremum over $V \in \mathcal{G}(s,d)$. The same type of estimate leads to (3.33). The formula in (3.34) follows by adapting the proof of Theorem 3.7. For the quantities $\overline{\theta}_{[1]}(V)$ from (3.34) we show

$$\overline{\theta}_{[1]}(\mathcal{R}(P^s_{0,i})) \leq \max\left(\overline{\theta}_{[1]}(\mathcal{W}^i_0), \overline{\theta}_{[1]}(\mathcal{R}(P^s_{0,i+1}))\right), \quad i = 1, \dots, \ell. \tag{3.36}$$

The estimate (3.30) for $v \in \mathcal{R}(P^s_{0,i}) \setminus (\mathcal{R}(P^s_{0,i+1}) \cup \mathcal{W}^i_0)$ now reads

$$\frac{1}{n} a_{k+1,k+n}(v) \leq \frac{1}{n} \left[C + a_{k+1,k_\star-j_\star-1}(P^s_{0,i+1}v) + a_{\max(k,k_\star+j_\star+1),n+k}(P^u_{0,i+1}v)\right].$$

Recall $a_{m,n} = 0$ for $m > n$ and note that there is no relation between $k, k_\star(v)$ and n. The condition (3.31) for n_0 turns into

$$\begin{aligned}\frac{1}{n} \sup_{v\in\mathcal{W}^i_0} \sup_{k\in\mathbb{N}_0} a_{k+1,k+n}(v) &\leq \overline{\theta}_{[1]}(\mathcal{W}^i_0) + \varepsilon, \quad \forall n \geq n_0, \\ \frac{1}{n} \sup_{v\in\mathcal{R}(P^s_{0,i+1})} \sup_{k\in\mathbb{N}_0} a_{k+1,k+n}(v) &\leq \overline{\theta}_{[1]}(\mathcal{R}(P^s_{0,i+1})) + \varepsilon, \quad \forall n \geq n_0.\end{aligned}$$

This leads to

$$\begin{aligned} a_{k_1,n+k}(P^u_{0,i+1}v) &\leq \begin{cases} (n+k-k_1)(\overline{\theta}_{[1]}(\mathcal{W}^i_0) + \varepsilon), & \text{if } n+k-k_1 \geq n_0, \\ n_0 \tfrac{\pi}{2}, & \text{if } n+k-k_1 < n_0, \end{cases} \\ a_{k+1,k_2}(P^s_{0,i+1}v) &\leq \begin{cases} (k_2-k-1)(\overline{\theta}_{[1]}(\mathcal{R}(P^s_{0,i+1})) + \varepsilon), & \text{if } k_2-k-1 \geq n_0, \\ n_0 \tfrac{\pi}{2}, & \text{if } k_2-k-1 < n_0, \end{cases} \end{aligned} \tag{3.37}$$

where $k_1 = \max(k, k_\star + j_\star + 1)$, $k_2 = k_\star - j_\star - 1$. In both cases $k \geq k_\star + j_\star + 1$ and $k < k_\star + j_\star + 1$ we find the estimate $n + k - k_1 + k_2 - k - 1 \leq n$ for the sum of coefficients in (3.37). Hence, we can continue

$$\frac{1}{n} a_{k+1,k+n}(v) \leq \frac{1}{n} \left[C + n_0\pi + n\left(\max(\overline{\theta}_{[1]}(\mathcal{W}^i_0), \overline{\theta}_{[1]}(\mathcal{R}(P^s_{0,i+1}))) + \varepsilon\right)\right].$$

Taking the supremum over k and v and then letting $n \to \infty$ yields the assertion (3.36) as in the proof of Theorem 3.7. ∎

4. Numerical algorithms and results. The aim of this section is to develop an algorithm for the numerical detection of outer angular values. The previous section provides the essential reduction result in Theorem 3.6:

$$\begin{aligned}\hat{\theta}_s &= \sup_{V\in\mathcal{G}(s,d)} \limsup_{n\to\infty} \frac{1}{n}\sum_{j=1}^{n} \measuredangle(\Phi(j-1,0)V, \Phi(j,0)V) \\ &= \sup_{V\in\mathcal{D}_0(s,d)} \limsup_{n\to\infty} \frac{1}{n}\sum_{j=1}^{n} \measuredangle(\Phi(j-1,0)V, \Phi(j,0)V).\end{aligned}$$

The search for the supremum of V in $\mathcal{D}_0(s,d)$ instead of $\mathcal{G}(s,d)$ reduces the computational effort substantially and, in some cases, one needs to consider only finitely many subspaces. This reduction method receives further support from the fact that some obvious numerical approaches tend to fail:

- Algorithms based on a simple forward iteration cannot provide the largest angular value. A generic subspace is pushed by the dynamics towards the most unstable trace space of equal dimension, see the upper row in Figure 3.4. But in general, the angular value is not achieved in this subspace. For the correct angular value, also non-generic subspaces must be considered, as sketched in the lower row of Figure 3.4. We refer to the Hénon example in Section 4.2.4 and to Figure 4.4 which illustrates the failure of a naive approach.
- Algorithms based on the computation of eigenvalues and eigenspaces, e.g. by applying the Schur decomposition, provide good results for autonomous systems. This fits well to our theory, since in the autonomous case, spectral bundles w.r.t. the dichotomy spectrum are indeed eigenspaces. The corresponding analysis for autonomous systems is carried out in detail in [9]. For nonautonomous models, eigenvalues of linearizations at a fixed time are known to be dynamically irrelevant as was first shown by Vinograd; see [36]. Corresponding algorithms fail in testing all trace subspaces.

To resolve these issues, we first detect the dichotomy spectrum and the corresponding spectral bundles. Then all trace subspaces become available, resulting in a numerically expensive but reliable approximation of $\hat{\theta}_s$. Finally, let us emphasize that this value aims at finding the subspace of maximal rotation in the global attractor of the system (if it exists). In general, our approach to angular values ignores other dynamically relevant features of the system, such as invariant manifolds or unstable fixed points and unstable periodic orbits if they do not belong to the ω-limit set of the current trajectory.

4.1. An algorithm for computing angular values. Consider the difference equation (1.1) on an interval $\mathbb{I}$ that is bounded from below. We propose the following three steps for the numerical approximation of $\hat{\theta}_s$.

First, we compute the dichotomy spectrum in step 1 followed by an approximation of the corresponding fiber bundles in step 2. To obtain accurate numerical results on the discrete interval $[0,M]\cap\mathbb{N}_0$, buffer intervals of length b (we choose $b=50$) are needed. The algorithm from [20, 25] requires to solve least squares problems on the extended interval $\mathbb{I}=[-b,M+b]\cap\mathbb{N}_0$.

The crucial part of our algorithm is the approximation of $\hat{\theta}_s$ for $s\in\{1,2\}$ in step 3. It is based on the reduction results from Section 3 and therefore needs the spectral bundles

that are computed in step 2. Readers, familiar with the computation of dichotomy spectra and spectral bundles may proceed directly with step 3.

Step 1: Computation of the dichotomy spectrum. The computation of Bohl exponents leads to an efficient algorithm for the approximation of the dichotomy spectrum. Upper and lower Bohl exponents of the scalar difference equation

$$u_{n+1} = a_n u_n, \quad n \in \mathbb{I}, \quad 0 < \inf_{n\in\mathbb{I}} |a_n| \le \sup_{n\in\mathbb{I}} |a_n| < \infty$$

are defined as, see [26]

$$\underline{\beta}(a_{\mathbb{I}}) := \lim_{n\to\infty} \inf_{\kappa\in\mathbb{I}} \left(\prod_{j=\kappa}^{\kappa+n-1} |a_j| \right)^{\frac{1}{n}}, \qquad \overline{\beta}(a_{\mathbb{I}}) := \lim_{n\to\infty} \sup_{\kappa\in\mathbb{I}} \left(\prod_{j=\kappa}^{\kappa+n-1} |a_j| \right)^{\frac{1}{n}}.$$

It follows that $\Sigma_{\mathrm{ED}} = [\underline{\beta}(a_{\mathbb{I}}), \overline{\beta}(a_{\mathbb{I}})]$.

For the d-dimensional difference equation (1.1), a corresponding result is more delicate to obtain. One may first transform the system into upper triangular form, using a `qr`-decomposition $A = QT$ of a given matrix A into the product of an orthogonal matrix Q and an upper triangular matrix T, see [24, Section 4.4] and [15]:

$$\begin{aligned} &Q_0 T_0 = \mathtt{qr}(A_0) \\ &\textbf{for } j = 1, 2, \dots \textbf{ do} \\ &\quad Q_j T_j = \mathtt{qr}(A_j Q_{j-1}) \\ &\textbf{end for} \end{aligned}$$

Note that $A_j = Q_j T_j Q_{j-1}^{\top}$ for $j \ge 1$. For non-degenerate models, the Bohl exponents of the diagonal entries of T_j (denoted by $T_j(i,i)$) determine the dichotomy spectrum. We refer to [33] for details on the corresponding theoretical background. More relations of Bohl exponents to other exponents and a perturbation analysis may be found for discrete-time systems in [6] and for continuous-time systems in [7]. In our case we fix a sufficiently large $H \in \mathbb{N}$ (called the Steklov window) and compute

$$\beta(i,\kappa) := \left(\prod_{j=\kappa}^{\kappa+H} |T_j(i,i)| \right)^{\frac{1}{H}}, \quad i = 1, \dots, d, \quad \kappa = 0, 1, \dots. \tag{4.1}$$

With $\underline{\beta}(i) := \min_\kappa \beta(i,\kappa)$, $\overline{\beta}(i) := \max_\kappa \beta(i,\kappa)$ we obtain the approximate spectrum $\Sigma_{\mathrm{ED}} \approx \bigcup_{i=1}^{d} [\underline{\beta}(i), \overline{\beta}(i)]$ where the values are ordered according to $\underline{\beta}(1) \ge \dots \ge \underline{\beta}(d)$. In the numerical experiments the spectral values turned out to be rather insensitive to the choice of Steklov window, and $H = \lfloor \frac{M}{2} \rfloor$ was found to be suitable for all results below.

Step 2: Computation of spectral bundles. Recall for $j \in \mathbb{N}$ and $i \in \{1, \dots, \ell\}$ the representation (3.4), (3.6) of the spectral bundle $\mathcal{W}_j^i = \mathcal{R}(\mathcal{P}_{j,i}) = \mathcal{R}(P_{j,i}^s P_{j,i+1}^u)$ with $\dim(\mathcal{W}_j^i) = d_i$. For computing these sets numerically, we apply the ansatz, proposed in [25, Section 2.5]. Take d_i random vectors $r_\nu \in \mathbb{R}^d$ and obtain a basis of $\mathcal{W}_j^i$ (in a generic sense) by calculating $\mathcal{P}_{j,i} r_\nu$ for $\nu = 1, \dots, d_i$. For this task, we choose $\gamma_i \in R_i$, $\gamma_{i+1} \in R_{i+1}$ close to the boundary of the spectral interval $\mathcal{I}_i$, cf. [25, Section 2.6]. We solve for each

$\nu \in \{1, \dots, d_i\}$ and simultaneously for $j \in [0, M] \cap \mathbb{N}_0$ the inhomogeneous linear systems

$$
\begin{aligned}
v_{n+1}^\nu &= \frac{1}{\gamma_{i+1}} A_n v_n^\nu + \delta_{n,j-1} r_\nu, \\
u_{n+1}^\nu &= \frac{1}{\gamma_i} A_n u_n^\nu - \delta_{n,j-1} A_{j-1} v_{j-1}^\nu,
\end{aligned}
\qquad n = -b, \dots, M+b-1 \tag{4.2}
$$

in a least squares sense. Here, δ denotes the Kronecker symbol. For the solutions of (4.2) one has $\mathcal{P}_{j,i} r_\nu \approx u_j^\nu$, and we refer to [25, Section 2.6] for precise error estimates. In this way, we obtain bases of $\mathcal{W}_j^i$ for $j \in [0, M] \cap \mathbb{N}_0$ and $i \in \{1, \dots, \ell\}$. If these fiber bundles are two-dimensional, we choose an orthonormal basis at each time instance. Note that an accurate computation of $\Phi(j, 0)v$ in (4.3) for $v \in \mathcal{B}_0^i$ can only be achieved by projecting the results to the respective spectral bundles. Thus, it does not suffice to have an approximation of the initial fiber $\mathcal{W}_0^i$, only.

Step 3: Computation of angular values. Assume that the spectral bundles $\mathcal{W}_j^i$, $i = 1, \dots, \ell$, $j = 0, \dots, M$ have been computed in step 2. We present a numerical scheme for computing approximate values of $\hat{\theta}_s$ in the case $s \in \{1, 2\}$. Assume $\dim(\mathcal{W}_0^i) \in \{1, 2\}$ and introduce the balls $\mathcal{B}_0^i = \{v \in \mathcal{W}_0^i : \|v\| = 1\}$ for all $i \in \{1, \dots, \ell\}$. For a subspace $V \in \mathcal{G}(s, d)$ (resp. a vector $v \in \mathbb{R}^d$) we abbreviate as in (2.4)

$$
\theta_s(V) = \frac{1}{M} a_{1,M}(V) = \frac{1}{M} \sum_{j=1}^{M} \measuredangle(\Phi(j-1, 0)V, \Phi(j, 0)V), \quad \theta_s(v) = \theta_s(\operatorname{span}(v)). \tag{4.3}
$$

Our goal is to use the M-dependent values $\theta_s(V)$ for an approximation of

$$
\hat{\theta}_s \approx \hat{\theta}_{s,M} := \sup_{V \in \mathcal{G}(s,d)} \theta_s(V). \tag{4.4}
$$

Starting with $s = 1$ our scheme reads:

for $i = 1, \dots, \ell$ **do**
  $w^i = \max_{v \in \mathcal{B}_0^i} \theta_1(v)$
end for
$\hat{\theta}_1 = \max_{i=1,\dots,\ell} w^i$.

If $\dim(\mathcal{W}_0^i) = 1$ then $\theta_1(\mathcal{W}_0^i)$ is computed for a single one-dimensional subspace. The detection of $\max_{v \in \mathcal{B}_0^i} \theta_1(v)$ is a one-dimensional optimization problem if $\dim \mathcal{W}_0^i = 2$. For this task, we apply the MATLAB-routine `fminbnd` that is based on golden section search and parabolic interpolation. The corresponding scheme for $s = 2$ is given by:

$\kappa = 0$
for $i = 1, \ldots, \ell$ **do**
  if $\dim(\mathcal{W}_0^i) = 2$ **then**
    $\kappa = \kappa + 1$
    $w^\kappa = \theta_2(\mathcal{W}_0^i)$
  end if
end for
for $i_1 = 1, \ldots, \ell - 1$ **do**
  for $i_2 = i_1 + 1, \ldots, \ell$ **do**
    $\kappa = \kappa + 1$
    $w^\kappa = \max_{x \in \mathcal{B}_0^{i_1}, y \in \mathcal{B}_0^{i_2}} \theta_2(\mathrm{span}(x, y))$
  end for
end for
$\hat{\theta}_2 = \max_{i=1,\ldots,\kappa} w^i$.

Note that the algorithm avoids to distinguish cases. If $\dim(\mathcal{W}_0^{i_1}) = \dim(\mathcal{W}_0^{i_2}) = 1$ then $\theta_2(\mathcal{W}_0^{i_1} \oplus \mathcal{W}_0^{i_2})$ is computed for a single two-dimensional subspace. In the case $\dim(\mathcal{W}_0^{i_1}) + \dim(\mathcal{W}_0^{i_2}) = 3$, we solve a one-dimensional optimization problem with the tools, described in the case $s = 1$. If $\dim(\mathcal{W}_0^{i_1}) + \dim(\mathcal{W}_0^{i_2}) = 4$, then the optimization problem is two-dimensional, and we apply the MATLAB-command `fminsearch`, which uses a derivative-free method for finding minima of unconstrained multivariable functions.

In all cases, we avoid numerical errors during the iteration of $\Phi(j, 0)x$ for $x \in \mathcal{W}_0^i$ (i.e. convergence towards the most unstable direction) by renormalizing the resulting output to $\mathcal{W}_j^i$ after each step.

4.2. Numerical experiments. We apply our algorithm from Section 4.1 to several models. First we reconsider some autonomous difference equations from cf. [9]. For this class of systems the algorithm from [9, Section 6] uses a series of Schur decompositions and one-dimensional optimization if necessary. Although this is more efficient for autonomous systems, we still apply in the following our general algorithm to the autonomous case in order to illustrate its performance. Furthermore, we apply both algorithms in Section 4.2.2 to autonomous systems and compare the results.

4.2.1. Two-dimensional models. We begin with several two-dimensional models for which angular values are analytically known. For these examples we always find point spectrum which we approximate by upper and lower Bohl exponents. In some cases upper and lower exponents coincide up to machine accuracy, while in other models, we numerically observe intervals of length $\approx 10^{-3}$. In the following we denote by $T_\varphi = \begin{pmatrix} \cos\varphi & -\sin\varphi \\ \sin\varphi & \cos\varphi \end{pmatrix}$ a rotation matrix.

The models from the first two rows in Table 4.1 are autonomous and we obtain approximately the expected results, see [9]. The second example is a reflection which exhibits the angular value $\hat{\theta}_1 = \frac{\pi}{2}$ with a somewhat smaller error. The third model is constructed via a nonautonomous similarity transformation with rotation matrices, and we obtain the angular value $\hat{\theta}_1 = \varphi = \frac{1}{3}$ with high accuracy. Finally, in the last row of Table 4.1 we consider a rotation by the angle $\varphi = \frac{1}{3}$ which is an irrational multiple of π. The angle $\measuredangle(u, T_{n \cdot \varphi} u)$ is $\frac{\pi}{4}$ on average, in agreement with our numerical experiment.

A_n	spectral intervals	$\hat{\theta}_{1,\mathrm{num}}$	$\lvert\hat{\theta}_1 - \hat{\theta}_{1,\mathrm{num}}\rvert$
$\left(\begin{smallmatrix} 2 & 0 \\ 0 & 3 \end{smallmatrix}\right)$	$\mathcal{I}_1 = [3,3]$ $\mathcal{I}_2 = [2,2]$	$5 \cdot 10^{-15}$	$5 \cdot 10^{-15}$
$\left(\begin{smallmatrix} \cos\varphi & \sin\varphi \\ \sin\varphi & -\cos\varphi \end{smallmatrix}\right)$	$\mathcal{I}_1 = [1,1]$	$\frac{\pi}{2} - 3{\cdot}10^{-5}$	$3 \cdot 10^{-5}$
$T_{(n+1)\varphi} \cdot \left(\begin{smallmatrix} 2 & 0 \\ 0 & 3 \end{smallmatrix}\right) \cdot T_{-n\cdot\varphi}$	$\mathcal{I}_1 = [2.996, 3.000]$ $\mathcal{I}_2 = [2.000, 2.002]$	$\frac{1}{3} + 6{\cdot}10^{-13}$	$6 \cdot 10^{-13}$
$T_{n\cdot\varphi}$	$\mathcal{I}_2 = [1,1]$	$\frac{\pi}{4} + 3.1{\cdot}10^{-4}$	$3.1 \cdot 10^{-4}$

Table 4.1: Spectral intervals and the first angular value for four examples. We set $\varphi = \frac{1}{3}$ and use our algorithm with $M = 2000$ iterates.

4.2.2. Two autonomous examples. Next we apply our algorithm to autonomous examples and compare with the output of [9, Algorithm 6.2] based on Schur decompositions. For this task we take the normal form

$$A(\rho,\varphi) = \begin{pmatrix} \cos(\varphi) & -\rho^{-1}\sin(\varphi) \\ \rho\sin(\varphi) & \cos(\varphi) \end{pmatrix}, \quad 0 < \rho \le 1, \quad 0 < \varphi \le \frac{\pi}{2} \tag{4.5}$$

and consider first the matrix $A(\frac{1}{7}, \frac{1}{3})$. The autonomous algorithm uses an in-depth analysis of the first angular value of (4.5), given in [9, Theorem 6.1]. The resulting angular value is $\hat{\theta}_{1,\mathrm{auto}} = 0.32106$. In coincidence with this result, the algorithm from Section 4.1 yields the spectral interval $\mathcal{I}_1 = [0.9991, 1.0009]$ and the angular value $\hat{\theta}_{1,\mathrm{num}} = 0.32175$.

Next, we analyze the four-dimensional matrix

$$A = \begin{pmatrix} A(1,\frac{1}{2}) & I_2 \\ 0 & \eta A(\frac{1}{2}, 1.4) \end{pmatrix}$$

with $\eta = 1.2$. This example is crucial since the angular values cannot be read off from the diagonal blocks only. Rather, one has to compute orthogonal bases of both two-dimensional invariant subspaces. The analysis and the corresponding algorithm in [9, Section 6.3.2] provide the angular value $\hat{\theta}_{1,\mathrm{auto}} = 1.355003$. Our current algorithm from Section 4.1 findes the spectral intervals

$$\mathcal{I}_1 = [1.1992, 1.2008] \quad \text{and} \quad \mathcal{I}_2 = [1.0000, 1.0000]$$

with corresponding angular values

$$\hat{\theta}_{1,\mathrm{num}} = \theta_1(\mathcal{W}_0^1) = 1.355095 \quad \text{and} \quad \theta_1(\mathcal{W}_0^2) = 0.500000.$$

This fits well to the results of the autonomous algorithm.

4.2.3. Angular values and tangent spaces. For a geometric interpretation of angular values, we consider an invertible discrete-time dynamical system defined on $\mathbb{Z}$. Let $F_n : \mathbb{R}^d \to \mathbb{R}^d$, $n \in \mathbb{Z}$ be a family of $\mathcal{C}^2$- diffeomorphisms and let

$$x_{n+1} = F_n(x_n), \quad n \in \mathbb{Z}. \tag{4.6}$$

Denote by Ψ the solution operator of (4.6). For a bounded trajectory $\xi_{\mathbb{Z}} := (\xi_n)_{n\in\mathbb{Z}}$, we introduce the corresponding variational equation

$$u_{n+1} = DF_n(\xi_n)u_n, \quad n \in \mathbb{Z}, \tag{4.7}$$

with solution operator Φ. Note that (4.6) has the form (1.1) with $A_n = DF_n(\xi_n)$. We further assume that the bounded trajectory $\xi_{\mathbb{Z}}$ is hyperbolic, i.e. 1 is in the resolvent set of the dichotomy spectrum of (4.7).

Stable and unstable fiber bundles of $\xi_{\mathbb{Z}}$ are defined at time $k \in \mathbb{Z}$ as

$$\mathcal{F}_k^s := \left\{ x \in \mathbb{R}^d : \lim_{n\to\infty} |\Psi(n,k)(x) - \xi_n| = 0 \right\},$$
$$\mathcal{F}_k^u := \left\{ x \in \mathbb{R}^d : \lim_{n\to-\infty} |\Psi(n,k)(x) - \xi_n| = 0 \right\},$$

and we denote corresponding tangent spaces by $T_{\xi_k}\mathcal{F}_k^s$ and $T_{\xi_k}\mathcal{F}_k^u$. These tangent spaces are related to spectral bundles from Section 3.1 as follows. Fix $i \in \{1,\dots,\ell\}$ such that $1 \in R_i$, where R_i denotes the i-th resolvent interval. We conclude from [32, Theorem 4.6.4] and (3.5) that

$$T_{\xi_k}\mathcal{F}_k^s = \mathcal{R}(P_{k,i}^s) = \bigoplus_{j=i}^{\ell} \mathcal{W}_k^j \quad \text{and} \quad T_{\xi_k}\mathcal{F}_k^u = \mathcal{R}(P_{k,i}^u) = \bigoplus_{j=1}^{i-1} \mathcal{W}_k^j.$$

For two-dimensional systems with $\dim(\mathcal{F}_k^s) = \dim(\mathcal{F}_k^u) = 1$, we observe that

$$\theta_1(\mathcal{W}_0^2) = \frac{1}{M}\sum_{j=1}^{M} \measuredangle(\Phi(j-1,0)\mathcal{W}_0^2, \Phi(j,0)\mathcal{W}_0^2) = \frac{1}{M}\sum_{j=1}^{M} \measuredangle(T_{\xi_{j-1}}\mathcal{F}_{j-1}^s, T_{\xi_j}\mathcal{F}_j^s),$$
$$\theta_1(\mathcal{W}_0^1) = \frac{1}{M}\sum_{j=1}^{M} \measuredangle(\Phi(j-1,0)\mathcal{W}_0^1, \Phi(j,0)\mathcal{W}_0^1) = \frac{1}{M}\sum_{j=1}^{M} \measuredangle(T_{\xi_{j-1}}\mathcal{F}_{j-1}^u, T_{\xi_j}\mathcal{F}_j^u)$$

describes the angle between successive stable resp. unstable tangent spaces on average. The maximum of these two averages is $\hat{\theta}_1 = \max\{\theta_1(\mathcal{W}_0^1), \theta_1(\mathcal{W}_0^2)\}$.

In higher dimensional systems, a geometric interpretation of angular values is more involved. If a three-dimensional model, for example, satisfies $\dim(\mathcal{F}_k^u) = 1$ and $\dim(\mathcal{F}_k^s) = 2$, we get for the one-dimensional unstable subspace

$$\theta_1(\mathcal{W}_0^1) = \frac{1}{M}\sum_{j=1}^{M} \measuredangle(T_{\xi_{j-1}}\mathcal{F}_{j-1}^u, T_{\xi_j}\mathcal{F}_j^u).$$

Next, we consider the two-dimensional stable subspace

$$\mathcal{W}_0^s := \begin{cases} \mathcal{W}_0^2, & \text{if } \dim(\mathcal{W}_0^2) = 2, \\ \mathcal{W}_0^2 \oplus \mathcal{W}_0^3, & \text{otherwise.} \end{cases}$$

The first angular value

$$\theta_1(\mathcal{W}_0^s) = \sup_{v\in T_{\xi_0}\mathcal{F}_0^s} \frac{1}{M}\sum_{j=1}^{M} \measuredangle(\Phi(j-1,0)v, \Phi(j,0)v)$$

describes on average the maximal angle between successive one-dimensional subspaces in $T_{\xi_{\mathbb{Z}}}\mathcal{F}^s_{\mathbb{Z}}$. Combining these result gives $\hat{\theta}_1 = \max\{\theta_1(\mathcal{W}^1_0), \theta_1(\mathcal{W}^s_0)\}$.

For three-dimensional models, also second angular values are of interest. The average angle between successive two-dimensional stable subspaces is given by

$$\theta_2(\mathcal{W}^s_0) = \frac{1}{M}\sum_{j=1}^{M} \measuredangle(T_{\xi_{j-1}}\mathcal{F}^s_{j-1}, T_{\xi_j}\mathcal{F}^s_j)$$

and the latter formula provides a nice geometrical interpretation. However, for computing $\hat{\theta}_2$, we have to consider further subspaces:

$$\hat{\theta}_2 = \max(\{\theta_2(\mathcal{W}^s_0)\} \cup \{\theta_2(V) : V = \mathcal{W}^1_0 \oplus \operatorname{span}(u) : u \in \mathcal{W}^s_0\}).$$

As a consequence, second and higher angular values are in general not achieved within the stable resp. unstable tangent bundle.

4.2.4. Models of Hénon type. We illustrate the geometric interpretation of angular values from Section 4.2.3 with two autonomous, nonlinear systems. Of interest are the two-dimensional Hénon map [22] as well as its three dimensional variant

$$F^2\begin{pmatrix} x_1 \\ x_2 \end{pmatrix} = \begin{pmatrix} 1 + x_2 - 1.4x_1^2 \\ 0.3x_1 \end{pmatrix}, \quad F^3\begin{pmatrix} x_1 \\ x_2 \\ x_3 \end{pmatrix} = \begin{pmatrix} 1 + x_3 - 1.4x_1^2 \\ x_1 + x_3 \\ 0.2x_1 + 0.1x_2 \end{pmatrix}.$$

The latter model is constructed similar to [10, Example 2], and possesses, like the original Hénon map, a non-trivial attractor.

We choose $M = 2000$ and compute angular values for the corresponding variational equation (4.7). Note that we apply the algorithm to these models even though we do not know whether the hyperbolicity assumptions are satisfied.

The two-dimensional Hénon model. We choose the initial point close to the Hénon attractor $\xi_{-50} = \begin{pmatrix} 0.7555 & 0.1671 \end{pmatrix}^\top$ and obtain the spectral intervals

$$\mathcal{I}_1 = [1.491, 1.549] \quad \text{and} \quad \mathcal{I}_2 = [0.194, 0.201]$$

with corresponding angular values

$$\theta_1(\mathcal{W}^1_0) = 0.3629, \quad \theta_1(\mathcal{W}^2_0) = 0.7506.$$

The maximum $\hat{\theta}_1 = \theta_1(\mathcal{W}^2_0)$ is achieved by the angle between successive stable tangent spaces. Stable and unstable tangent spaces are shown in Figure 4.1. In addition, we present approximations of the stable and of the unstable manifold of the fixed point ξ.

Figure 4.2 shows the dependence of $\hat{\theta}_{1,M}$ from (4.4) on the length M of the finite interval. We observe the typical slow convergence of the ergodic average (4.3) as $M \to \infty$. So far the approximate value $\hat{\theta}_{1,M}$ in (4.4) was computed by starting at time $k = 0$. It is instructive to compare these results with the values obtained from

$$\theta_1(k, M) := \sup_{V \in \mathcal{G}(1,2)} \frac{1}{M}\sum_{j=k+1}^{k+M} \measuredangle(\Phi(j-1, k)V, \Phi(j, k)V), \tag{4.8}$$

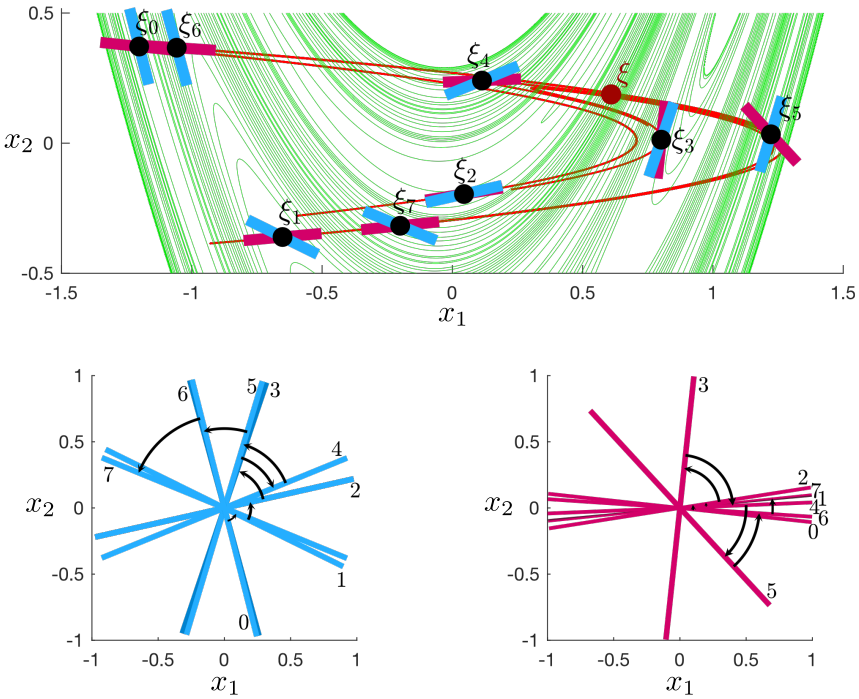

Figure 4.1: Upper panel: Stable (green) and unstable (red) manifolds of the fixed point ξ of the two-dimensional Hénon model. Lower panel: Successive stable (left) and unstable (right) tangent spaces.

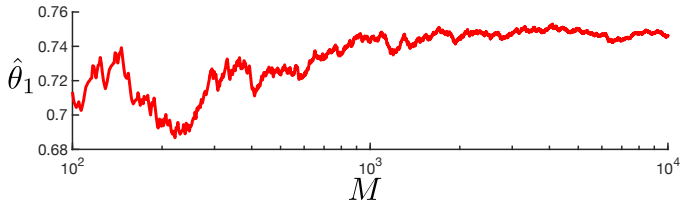

Figure 4.2: Angular value $\hat{\theta}_1$ in the two-dimensional Hénon model, computed for $M \in [10^2, 10^4] \cap \mathbb{N}$.

where the computation starts at a later time $k \in \mathbb{N}$. Taking the supremum over k results in an approximation of uniform outer angular values $\hat{\theta}_{[s]}$ from Definition 2.6. Here we analyze the dependence of (4.8) on $k \in \{0, \dots, 10^4\}$ for the values $M \in \{10^2, 10^3, 10^4\}$. Figure 4.3 shows the result for the two-dimensional Hénon model. The numerical data suggest convergence as $M \to \infty$ uniformly in k. However, we argue that we do not expect this to hold in theory for the following reason. Assume the orbit $(\xi_n)_{n \in \mathbb{Z}}$ is dense in the Hénon attractor, which contains the saddle fixed point and its unstable manifold. Then there exist arbitrarily long time intervals on which the orbit is close to the local unstable manifold. Thus, one finds arbitrarily large values of k for which $\theta_1(k, M)$ is close to 0. It will be extremely difficult to observe this non-uniformity w.r.t. k numerically since one needs k-values which grow exponentially with the observation length M.

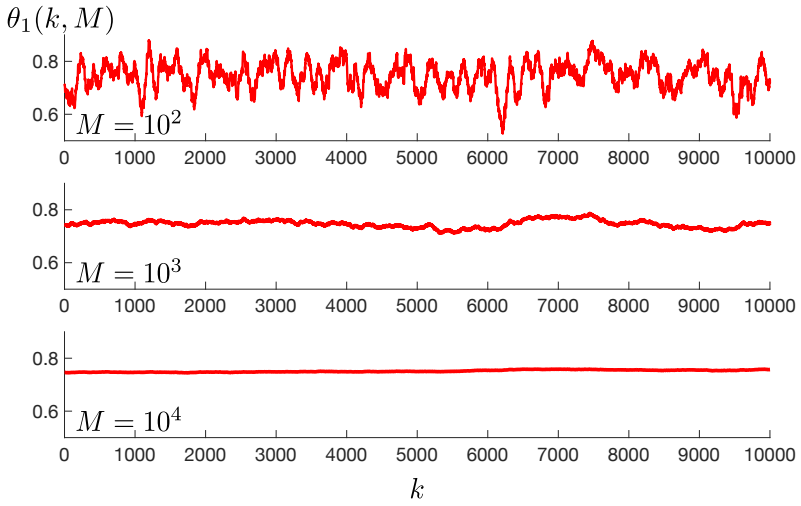

Figure 4.3: Computation of $\theta_1(k, M)$ for the two-dimensional Hénon map.

In the next experiment we show that a naive approach to compute the angular values by forward iteration tends to fail. We consider

$$\theta_1(V_\varphi) \quad \text{with} \quad V_\varphi = \operatorname{span} \begin{pmatrix} \cos(\varphi) \\ \sin(\varphi) \end{pmatrix}$$

for 10^5 equidistant values of $\varphi \in [0, \pi]$ and display the values $\theta_1(V_\varphi)$ from (4.3) with $M = 2000$ fixed, in Figure 4.4. As we know, the angular value $\hat{\theta}_1 = 0.7506$ is achieved by

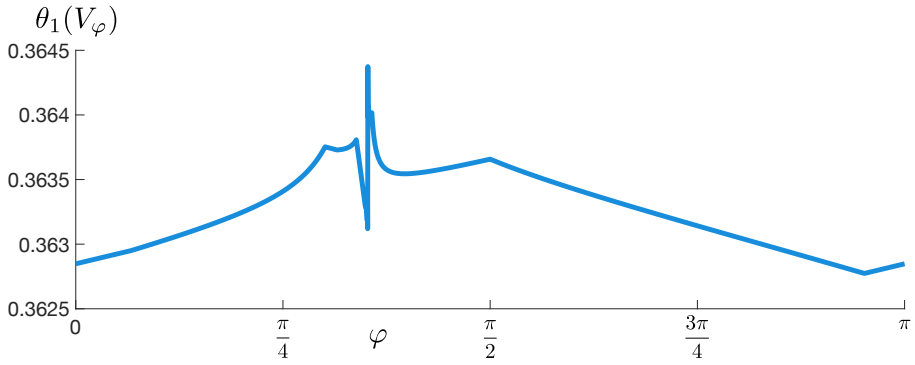

Figure 4.4: Computation of $\theta_1(V_\varphi)$ for the two-dimensional Hénon map for 10^5 values of $\varphi \in [0, \pi]$.

the tangent space to the stable fiber. However, each subspace V_φ with φ chosen from a very fine grid, is pushed during $M = 2000$ iterations towards the unstable subspace. The peak at $\varphi \approx 1.1$ indicates the appropriate stable subspace, but the observed maximum value is only slightly larger than $\theta_1(\mathcal{W}_0^1) = 0.3629 \ll 0.7506 = \hat{\theta}_1$.

The three-dimensional Hénon model. We choose $\xi_{-81} = \begin{pmatrix} 0.2 & 0.1 & 0 \end{pmatrix}^\top$ as initial point and obtain the spectral intervals

$$\mathcal{I}_1 = [1.406, 1.442], \quad \mathcal{I}_2 = [0.378, 0.387] \quad \text{and} \quad \mathcal{I}_3 = [0.318, 0.333].$$

The corresponding unstable fibers $\mathcal{W}_k^1 = T_{\xi_k}\mathcal{F}_k^u$ are one-dimensional and the direct sum of the stable fibers $\mathcal{W}_k^2 \oplus \mathcal{W}_k^3 = T_{\xi_k}\mathcal{F}_k^s$ is two-dimensional. These subspaces are shown in Figure 4.5 for $0 \le k \le 4$.

The angular value $\hat{\theta}_1 = 0.8129$ is achieved in $\mathcal{W}_0^1$:

$$\theta_1(\mathcal{W}_0^1) = 0.825, \quad \theta_1(\mathcal{W}_0^2) = 0.693, \quad \theta_1(\mathcal{W}_0^3) = 0.757.$$

While the first angular value $\hat{\theta}_1$ describes the angle between successive unstable tangent spaces $T_{\xi_k}\mathcal{F}_k^u$ on average, the average angle between successive stable tangent spaces $T_{\xi_k}\mathcal{F}_k^s$ is given by the second angular value $\hat{\theta}_2 = 0.839$, see Figure 4.5. This value is found as the maximum of the following numerical computations

$$\theta_2(\mathcal{W}_0^2 \oplus \mathcal{W}_0^3) = 0.839, \quad \theta_2(\mathcal{W}_0^1 \oplus \mathcal{W}_0^2) = 0.611, \quad \theta_2(\mathcal{W}_0^1 \oplus \mathcal{W}_0^3) = 0.703.$$

Note that generally, angular values are not achieved within stable respectively unstable subspaces. The three-dimensional Hénon model seems to be exceptional in this regard. In general, invariant subspaces (in a nonautonomous sense) in which angular values are achieved, are not characterized by contracting or expanding dynamics; see Section 4.2.3 and 4.2.5.

4.2.5. A three-dimensional toy model. We construct a three-dimensional nonautonomous model which depends on a parameter but has constant angular values. However, the parameter changes the spectrum and the stability properties as well as the spectral bundles. We show that the algorithm succeeds in finding the correct angular value regardless whether or not the optimization step is invoked.

With $\varphi = \frac{1}{3}$ and parameter $\lambda > 0$ the model has the form

$$A_n = T^{1,2}_{\varphi(n+52)} \cdot \begin{pmatrix} \frac{1}{2} & 0 & 0 \\ 0 & \lambda & 0 \\ 0 & 0 & 3 \end{pmatrix} \cdot T^{1,2}_{-\varphi(n+51)} \text{ with } T^{1,2}_{\varphi} = \begin{pmatrix} \cos\varphi & -\sin\varphi & 0 \\ \sin\varphi & \cos\varphi & 0 \\ 0 & 0 & 1 \end{pmatrix} \tag{4.9}$$

and point spectrum $\{\frac{1}{2}, \lambda, 3\}$. One can show that both angular values are independent of the parameter λ and satisfy $\hat{\theta}_1 = \hat{\theta}_2 = \varphi = \frac{1}{3}$. By choosing $\lambda = \frac{1}{2}$ and $\lambda = 2$ we vary the dimensions of the corresponding spectral bundles and study the consequences.

$\lambda = \frac{1}{2}$. The numerical spectral intervals are $\mathcal{I}_1 = [3, 3]$ and $\mathcal{I}_2 = [\frac{1}{2}, \frac{1}{2}]$, and we obtain the first angular value

$$\theta_1(\mathcal{W}_0^1) = 0, \quad \max_{x \in \mathcal{B}_0^2} \theta_1(x) = \frac{1}{3}, \quad \hat{\theta}_1 = \frac{1}{3},$$

and the second angular value

$$\theta_2(\mathcal{W}_0^2) = 0, \quad \max_{x \in \mathcal{B}_0^2} \theta_2(\mathcal{W}_0^1 \oplus \operatorname{span}(x)) = \frac{1}{3}, \quad \hat{\theta}_2 = \frac{1}{3},$$

cf. Figure 4.6. Note that the subspaces, in which the maximum is achieved are not unique. The component in $\mathcal{W}_0^2$ can be chosen arbitrarily.

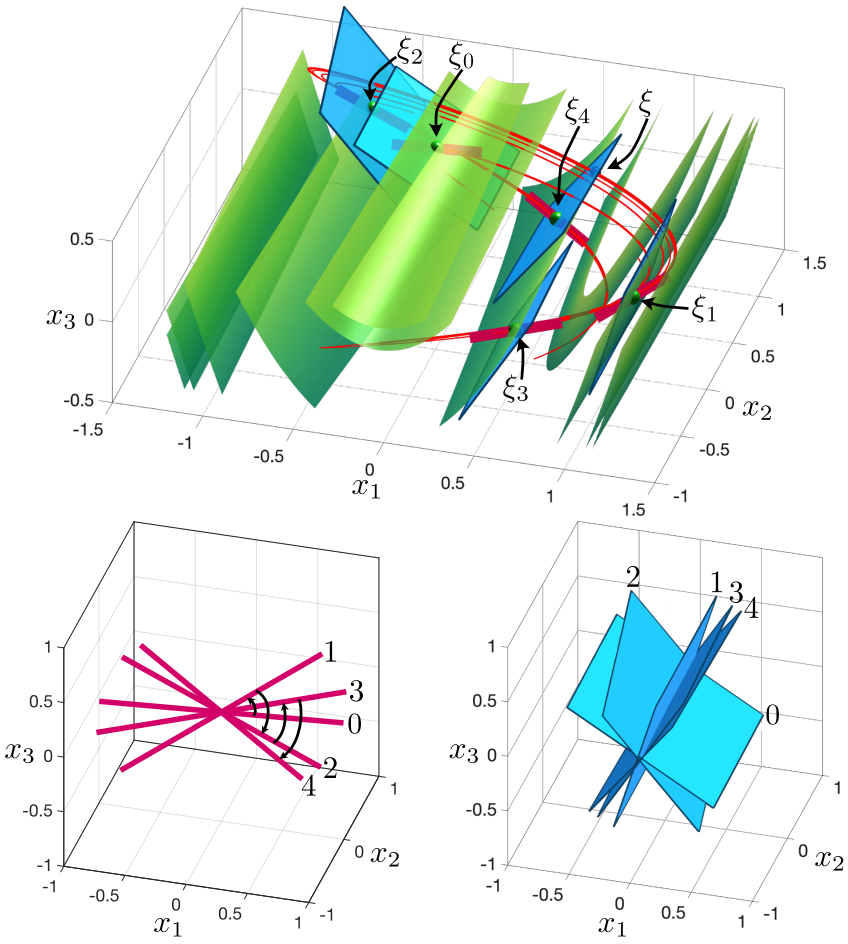

Figure 4.5: Upper panel: Stable (green) and unstable (red) manifolds of the fixed point ξ of the three-dimensional Hénon model. Lower panel: Successive one-dimensional unstable (left) and two-dimensional stable (right) tangent spaces.

$\lambda = 2$. In this example, we obtain three spectral intervals $\mathcal{I}_1 = [3, 3]$, $\mathcal{I}_2 = [1.9955, 2.0000]$ and $\mathcal{I}_3 = [0.5000, 0.5011]$. We find that

$$\theta_1(\mathcal{W}_0^1) = 0, \quad \theta_1(\mathcal{W}_0^2) = \frac{1}{3}, \quad \theta_1(\mathcal{W}_0^3) = \frac{1}{3}.$$

Thus $\hat{\theta}_1 = \frac{1}{3}$, where the maximum is achieved for two fibers. In Figure 4.7, the algorithm chooses $\mathcal{W}_0^3$. The second angular value is also achieved for two different trace spaces:

$$\theta_2(\mathcal{W}_0^1 \oplus \mathcal{W}_0^2) = \frac{1}{3}, \quad \theta_2(\mathcal{W}_0^1 \oplus \mathcal{W}_0^3) = \frac{1}{3}, \quad \theta_2(\mathcal{W}_0^2 \oplus \mathcal{W}_0^3) = 0, \quad \hat{\theta}_2 = \frac{1}{3}.$$

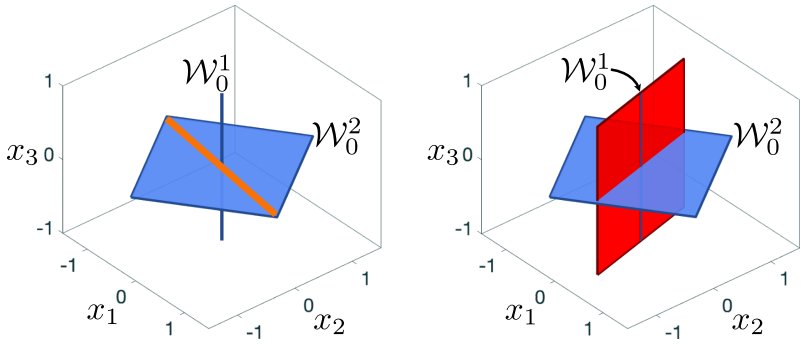

Figure 4.6: Spectral bundles (blue) of (4.9) for $\lambda = \frac{1}{2}$. The angular values $\hat{\theta}_{1,2}$ are achieved at subspaces which are shown in red.

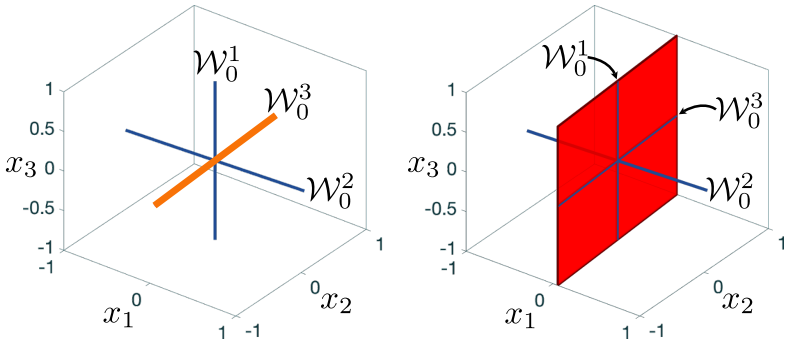

Figure 4.7: Spectral bundles (blue) of (4.9) for $\lambda = 2$. The angular values $\hat{\theta}_{1,2}$ are achieved at subspaces which are shown in red.

4.2.6. A random dynamical system. For $\varphi = 0.2$, we define

$$B_1 = \begin{pmatrix} 2\cos(\varphi) & -2\sin(\varphi) & 0 \\ 2\sin(\varphi) & 2\cos(\varphi) & 0 \\ 0 & 0 & 3 \end{pmatrix}, \quad B_2 = \begin{pmatrix} 1 & 0 & 0 \\ 0 & 1 & 0 \\ 0 & 0 & 5 \end{pmatrix}$$

and construct the 3-dimensional random dynamical system

$$A_n = B_r, \qquad \text{where } r \in \{1, 2\} \text{ is uniformly distributed for each } n \in \mathbb{I}.$$

This random dynamical system allows an explicit study of the dichotomy spectrum, see [1, Remark 4.2.9], and of angular values. One has $\Sigma_{\mathrm{ED}} = \{\lambda_1, \lambda_2\}$ with

$$\lambda_1 = \sqrt{3 \cdot 5} \approx 3.872, \quad \lambda_2 = \sqrt{1 \cdot 2} \approx 1.414$$

and the corresponding fiber bundles are

$$\mathcal{W}_0^1 = \operatorname{span} \begin{pmatrix} 0 \\ 0 \\ 1 \end{pmatrix}, \quad \mathcal{W}_0^2 = \operatorname{span} \left(\begin{pmatrix} 1 \\ 0 \\ 0 \end{pmatrix}, \begin{pmatrix} 0 \\ 1 \\ 0 \end{pmatrix} \right).$$

The first and second angular values are equal to 1, since

$$\theta_1(\mathcal{W}_0^1) = 0, \quad \forall x \in \mathcal{B}_0^2 : \theta_1(x) = \frac{0.2 + 0}{2} = 0.1$$

and

$$\theta_2(\mathcal{W}_0^2) = 0, \quad \forall x \in \mathcal{B}_0^2 : \theta_2(\mathcal{W}_0^1 \oplus \operatorname{span}(x)) = 0.1.$$

These analytic results are in coincidence with the output of our numerical algorithm. One realization gives the spectral intervals $\mathcal{I}_1 = [3.86, 3.92]$ and $\mathcal{I}_2 = [1.39, 1.42]$ and the first angular value

$$\theta_1(\mathcal{W}_0^1) = 0, \quad \max_{x \in \mathcal{B}_0^2} \theta_1(x) = 0.099631 = \hat{\theta}_1.$$

A numerical computation of the second angular value yields

$$\theta_2(\mathcal{W}_0^2) = 0, \quad \max_{x \in \mathcal{B}_0^2} \theta_2(\mathcal{W}_0^1 \oplus \operatorname{span}(x)) = 0.099631 = \hat{\theta}_2.$$

4.2.7. Coupled oscillators. We consider a canonical model for two nonlinear oscillators with a linear diffusion-like coupling originating from [3]. It has been frequently used as a model problem for analyzing and computing invariant tori [18, 16, 34]:

$$x' = G(x), \quad G(x) = \begin{pmatrix} x_1 + p_1 x_2 - (x_1^2 + x_2^2)x_1 - \lambda(x_1 + x_2 - x_3 - x_4) \\ -p_1 x_1 + x_2 - (x_1^2 + x_2^2)x_2 - \lambda(x_1 + x_2 - x_3 - x_4) \\ x_3 + p_2 x_4 - (x_3^2 + x_4^2)x_3 + \lambda(x_1 + x_2 - x_3 - x_4) \\ -p_2 x_3 + x_4 - (x_3^2 + x_4^2)x_4 + \lambda(x_1 + x_2 - x_3 - x_4) \end{pmatrix}. \tag{4.10}$$

For parameter values λ in some interval $[0, \lambda_{\text{crit}})$ the model possesses an invariant torus which breaks down at a critical value $\lambda_{\text{crit}} > 0$; see [17], [34] for a thorough analysis of this phenomenon and numerical results for $p_1 = p_2 = 0.55$ where $\lambda_{\text{crit}} \approx 0.2607$. It is worth noting that this system has a $\mathbb{Z}_2$-symmetry which can be written as $G(Sx) = SG(x), x \in \mathbb{R}^4$ for the permutation $S(x_1, x_2, x_3, x_4)^\top = (x_3, x_4, x_1, x_2)^\top$. In the following we consider the 1-flow $F : \mathbb{R}^4 \to \mathbb{R}^4$ of (4.10) which inherits the symmetry $S \circ F = F \circ S$. In particular, the symmetric space $X_s = \{x \in \mathbb{R}^4 : Sx = x\}$ and the antisymmetric space $X_a = \{x \in \mathbb{R}^4 : Sx = -x\}$ are invariant. As in Section 4.2.3 we determine angular values of the variational equation along an F-orbit. The 1-flow is approximated by the explicit Euler scheme which respects the symmetry. The following data are obtained with step size $h = 0.01$, and orbit length $M = 1000$. For 21 equidistant values of $\lambda \in [0.1, 0.3]$, we compute the first and second angular value in Figure 4.8. We choose for each value of λ a random initial point in $[-1, 1]^4$.

The breakdown of the invariant torus can be understood by comparing Lyapunov-type numbers which measure the contraction within the torus and toward the torus; see [17]. Angular values are not suitable for this task. They measure the maximal average rotation of one- and two-dimensional subspaces in an attractor of the system. In the coupled oscillator system almost all trajectories converge to the in-phase symmetric orbit (lying on the torus if it exists). Thus the spectral bundle consists of the Floquet spaces (including the flow direction) and the angular values represent the maximal rotation of one- or two dimensional subspaces composed of Floquet spaces. In case of an antisymmetric initial value (and since the computation preserves antisymmetry) the orbit converges towards the unstable antisymmetric periodic orbit (lying on the invariant torus if it exists). Then

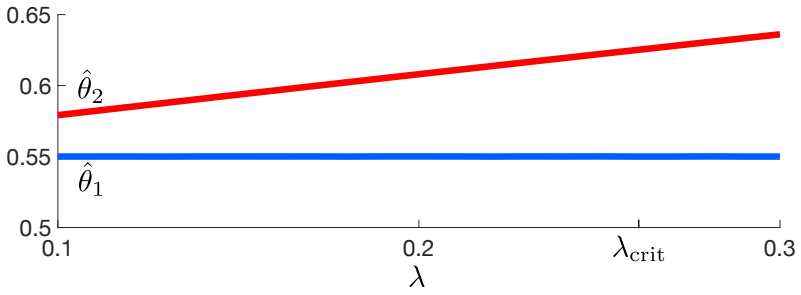

Figure 4.8: First (blue) and second angular value (red) for $\lambda \in [0.1, 0.3]$.

angular values measure the maximum rotation of Floquet subspaces belonging to this unstable orbit. For both initial data the corresponding angular value passes smoothly through the parameter domain where the torus breaks down. Close to the breakdown of the invariant torus, we compute two orbits for $\lambda = 0.26$ with antisymmetric initial value $x_a = (0.1, 1, -0.1, -1)^\top$ and nonsymmetric initial value $x_r = (0.1, 1, 0.2, 0.1)^\top$ at time -50, shown in Figure 4.9. Table 4.2 and 4.3 contain the corresponding spectral intervals and angular values. Note that one spectral interval always contains the trivial Floquet multiplier 1 and that the symmetric periodic orbit is orbitally stable while the antisymmetric one is unstable. The findings are in accordance with the results in [34]. The corresponding (Floquet-) subspaces at time 50 are depicted in Figure 4.10. It is worth noting that the 2D fibers $\mathcal{W}_0^1 \oplus \mathcal{W}_0^3$ and $\mathcal{W}_0^2 \oplus \mathcal{W}_0^4$ agree with the symmetric resp. the antisymmetric space. Their invariance ensures that the second angular value is zero as confirmed by the corresponding entries in Table 4.3.

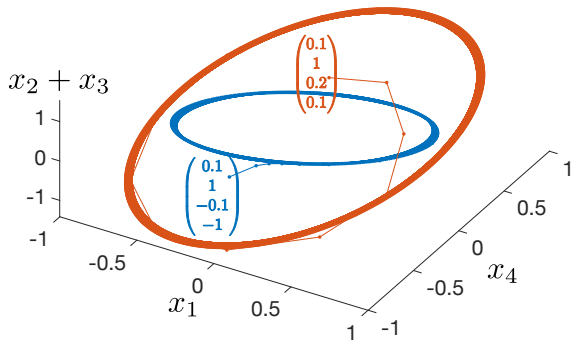

Figure 4.9: Two orbits for $\lambda = 0.26$ with antisymmetric and arbitrary initial value.

initial data	antisymmetric x_a		nonsymmetric x_r	
1D trace space	interval	θ_1	interval	θ_1
$\mathcal{W}_0^1$	$[1.186, 1.195]$	0.194	$[0.999, 1.000]$	0.550
$\mathcal{W}_0^2$	$[0.995, 1.005]$	0.179	$[0.621, 0.624]$	0.549
$\mathcal{W}_0^3$	$[0.902, 0.918]$	0.213	$[0.132, 0.133]$	0.550
$\mathcal{W}_0^4$	$[0.379, 0.383]$	0.179	$[0.074, 0.0749]$	0.550

Table 4.2: First angular values for the trace spaces ($\approx$ 1D Floquet spaces) of the orbits from Figure 4.9 converging to the antisymmetric resp. the symmetric periodic orbit. The maximum is $\hat{\theta}_1 = 0.213$ resp. $\hat{\theta}_1 = 0.550$.

initial data	antisymmetric x_a	nonsymmetric x_r
2D trace space	θ_2	θ_2
$\mathcal{W}_0^1 \oplus \mathcal{W}_0^2$	0.301	0.625
$\mathcal{W}_0^1 \oplus \mathcal{W}_0^3$	0.000	0.000
$\mathcal{W}_0^1 \oplus \mathcal{W}_0^4$	0.256	0.625
$\mathcal{W}_0^2 \oplus \mathcal{W}_0^3$	0.311	0.625
$\mathcal{W}_0^2 \oplus \mathcal{W}_0^4$	0.000	0.000
$\mathcal{W}_0^3 \oplus \mathcal{W}_0^4$	0.258	0.625

Table 4.3: Second angular value for the trace spaces ($\approx$ 2D Floquet spaces) of the orbits from Figure 4.9 converging to the antisymmetric resp. the symmetric periodic orbit. The maximum is $\hat{\theta}_2 = 0.311$ resp. $\hat{\theta}_2 = 0.625$

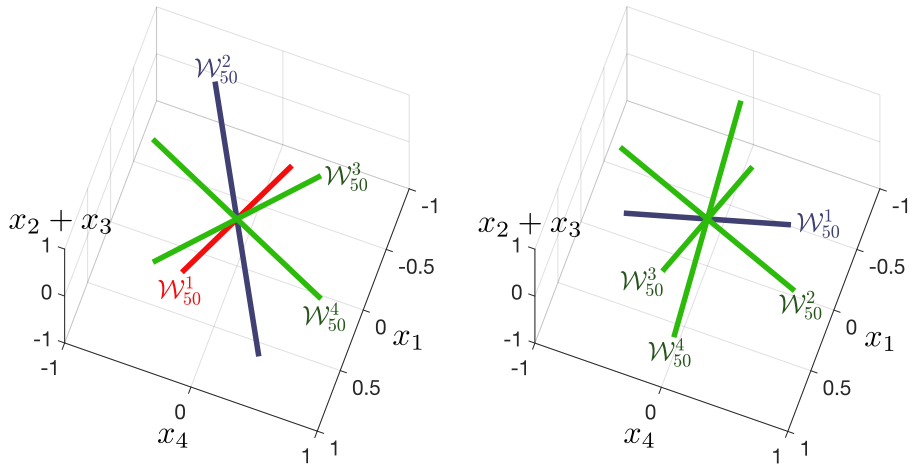

Figure 4.10: Spectral bundle of 4 subspaces ($\approx$ Floquet spaces) at time 50 for $\lambda = 0.26$ and antisymmetric (left) resp. nonsymmetric initial data (right). Coloring: green (stable), red (unstable), blue (neutral $\approx$ flow direction).

Acknowledgments. The authors thank Gary Froyland for valuable comments which led to improvements of this paper. Our thanks also go to an anonymous referee whose comments led to substantial clarifications, in particular in Section 4. Both authors are grateful to the Research Centre for Mathematical Modelling (RCM^2) at Bielefeld University for continuous support of their joint research. For further support, WJB thanks the CRC 1283 "Taming Uncertainty and Profiting from Randomness and Low Regularity in Analysis, Stochastics and Their Applications" and TH thanks the Faculty of Mathematics at Bielefeld University.

REFERENCES

[1] L. Arnold. *Random dynamical systems*. Springer Monographs in Mathematics. Springer-Verlag, Berlin, 1998.

[2] L. Arnold and L. San Martin. A multiplicative ergodic theorem for rotation numbers. *J. Dynam. Differential Equations*, 1(1):95–119, 1989.

[3] D. G. Aronson, E. J. Doedel, and H. G. Othmer. An analytical and numerical study of the bifurcations in a system of linearly-coupled oscillators. *Phys. D*, 25(1-3):20–104, 1987.

[4] B. Aulbach and J. Kalkbrenner. Exponential forward splitting for noninvertible difference equations. *Comput. Math. Appl.*, 42(3-5):743–754, 2001.

[5] B. Aulbach and S. Siegmund. The dichotomy spectrum for noninvertible systems of linear difference equations. *J. Differ. Equations Appl.*, 7:895–913, 2001.

[6] A. Babiarz, A. Czornik, M. Niezabitowski, E. Barabanov, A. Vaidzelevich, and A. Konyukh. Relations between Bohl and general exponents. *Discrete Contin. Dyn. Syst.*, 37(10):5319–5335, 2017.

[7] E. A. Barabanov and A. V. Konyukh. Bohl exponents of linear differential systems. *Mem. Differential Equations Math. Phys.*, 24:151–158, 2001.

[8] L. Barreira. *Lyapunov exponents*. Birkhäuser/Springer, Cham, 2017.

[9] W.-J. Beyn, G. Froyland, and T. Hüls. Angular values of nonautonomous and random linear dynamical systems: Part I—Fundamentals. *SIAM J. Appl. Dyn. Syst.*, 21(2):1245–1286, 2022.

[10] W.-J. Beyn and J.-M. Kleinkauf. Numerical approximation of homoclinic chaos. *Numer. Algorithms*, 14:25–53, 1997.

[11] W. A. Coppel. *Dichotomies in Stability Theory*. Springer, Berlin, 1978. Lecture Notes in Mathematics, Vol. 629.

[12] J. L. Daleckiĭ and M. G. Kreĭn. *Stability of Solutions of Differential Equations in Banach Space*. American Mathematical Society, Providence, R.I., 1974.

[13] W. de Melo and S. van Strien. *One-dimensional dynamics*, volume 25 of *Ergebnisse der Mathematik und ihrer Grenzgebiete (3)*. Springer-Verlag, Berlin, 1993.

[14] L. Dieci and C. Elia. The singular value decomposition to approximate spectra of dynamical systems. Theoretical aspects. *J. Differential Equations*, 230(2):502–531, 2006.

[15] L. Dieci, C. Elia, and E. Van Vleck. Exponential dichotomy on the real line: SVD and QR methods. *J. Differential Equations*, 248(2):287–308, 2010.

[16] L. Dieci and J. Lorenz. Computation of invariant tori by the method of characteristics. *SIAM J. Numer. Anal.*, 32(5):1436–1474, 1995.

[17] L. Dieci and J. Lorenz. Lyapunov-type numbers and torus breakdown: numerical aspects and a case study. volume 14, pages 79–102. 1997. Dynamical numerical analysis (Atlanta, GA, 1995).

[18] L. Dieci, J. Lorenz, and R. D. Russell. Numerical calculation of invariant tori. *SIAM J. Sci. Statist. Comput.*, 12(3):607–647, 1991.

[19] D. E. Edmunds and W. D. Evans. *Spectral theory and differential operators*. Oxford mathematical monographs. Clarendon Press, Oxford, repr. (with corr.), digital print. edition, 2002.

[20] G. Froyland, T. Hüls, G. P. Morriss, and T. M. Watson. Computing covariant Lyapunov vectors, Oseledets vectors, and dichotomy projectors: A comparative numerical study. *Phys. D*, 247:18–39, 2013.

[21] G. H. Golub and C. F. Van Loan. *Matrix computations*. Johns Hopkins Studies in the Mathematical Sciences. Johns Hopkins University Press, Baltimore, MD, fourth edition, 2013.

[22] M. Hénon. A two-dimensional mapping with a strange attractor. *Comm. Math. Phys.*, 50(1):69–77,

1976.
[23] D. Henry. *Geometric Theory of Semilinear Parabolic Equations*. Springer, Berlin, 1981.
[24] T. Hüls. Computing Sacker-Sell spectra in discrete time dynamical systems. *SIAM J. Numer. Anal.*, 48(6):2043–2064, 2010.
[25] T. Hüls. Computing stable hierarchies of fiber bundles. *Discrete Contin. Dyn. Syst. Ser. B*, 22(9):3341–3367, 2017.
[26] T. Hüls and C. Pötzsche. Qualitative analysis of a nonautonomous Beverton-Holt Ricker model. *SIAM J. Appl. Dyn. Syst.*, 13(4):1442–1488, 2014.
[27] S. Jiang. Angles between Euclidean subspaces. *Geom. Dedicata*, 63(2):113–121, 1996.
[28] J. Kalkbrenner. *Exponentielle Dichotomie und chaotische Dynamik nichtinvertierbarer Differenzengleichungen*, volume 1 of *Augsburger Mathematisch-Naturwissenschaftliche Schriften*. Dr. Bernd Wißner, Augsburg, 1994.
[29] A. B. Katok and B. Hasselblatt. *Introduction to the modern theory of dynamical systems*. Encyclopedia of mathematics and its applications ; vol. 54. Cambridge University Press, Cambridge, 1995.
[30] Z. Nitecki. *Differentiable dynamics. An introduction to the orbit structure of diffeomorphisms*. The M.I.T. Press, Cambridge, Mass.-London, 1971.
[31] O. Perron. Die Stabilitätsfrage bei Differentialgleichungen. *Math. Z.*, 32(1):703–728, 1930.
[32] C. Pötzsche. *Geometric theory of discrete nonautonomous dynamical systems*, volume 2002 of *Lecture Notes in Mathematics*. Springer-Verlag, Berlin, 2010.
[33] C. Pötzsche. Dichotomy spectra of triangular equations. *Discrete Contin. Dyn. Syst.*, 36(1):423–450, 2016.
[34] V. Reichelt. Computing invariant tori and circles in dynamical systems. In *Numerical methods for bifurcation problems and large-scale dynamical systems (Minneapolis, MN, 1997)*, volume 119 of *IMA Vol. Math. Appl.*, pages 407–437. Springer, New York, 2000.
[35] R. J. Sacker and G. R. Sell. A spectral theory for linear differential systems. *J. Differential Equations*, 27(3):320–358, 1978.
[36] R. E. Vinograd. On a criterion of instability in the sense of Lyapunov of the solutions of a linear system of ordinary differential equations. *Doklady Akad. Nauk SSSR (N.S.)*, 84:201–204, 1952.